Clinical Epigenetics

RESEARCH

Open Access

Maternal loss of mouse *Nlrp2* alters the transcriptome and DNA methylome in GV oocytes and impairs zygotic genome activation in embryos

Zahra Anvar[1,2], Michael D. Jochum[1,3], Imen Chakchouk[1,2], Momal Sharif[1,2], Hannah Demond[4,5,6,7], Alvin K. To[1], Daniel C. Kraushaar[8], Ying-Wooi Wan[1,2], Michael C. Mari[1,2], Simon Andrews[9], Gavin Kelsey[4,10,11] and Ignatia B. Van den Veyver[1,2,12*]

Abstract

Background NLRP2 is a subcortical maternal complex (SCMC) protein of mammalian oocytes and preimplantation embryos. SCMC proteins are encoded by maternal effect genes and play a pivotal role in the maternal-to-zygotic transition (MZT), early embryogenesis, and epigenetic (re)programming. Maternal inactivation of genes encoding SCMC proteins has been linked to infertility and subfertility in mice and humans, but the underlying molecular mechanisms for the diverse functions of SCMC proteins, and specifically the role of NLRP2, are incompletely understood.

Results We profiled the DNA methylome of pre-ovulatory germinal-vesicle (GV) oocytes from *Nlrp2*-null, heterozygous (Het), and wild-type (WT) female mice and assessed the transcriptome of GV oocytes and 2-cell embryos from WT and *Nlrp2*-null females. The absence or reduction of NLRP2 did not alter the distinctive global DNA methylation landscape of GV oocytes, including their unique bimodal methylome patterns and methylation at the germline differentially methylated regions (gDMRs) of imprinted genes. However, altered methylation was observed in a small subset of oocyte-characteristic hyper- and hypomethylated domains and within a minor fraction of genomic regions, particularly in *Nlrp2*-null oocytes. Transcriptome profiling revealed substantial differences between the *Nlrp2*-null and WT GV oocytes, including deregulation of many crucial factors involved in oocyte transcriptome modulation and epigenetic reprogramming. Moreover, maternal absence of NLRP2 significantly altered the transcriptome of heterozygous embryos from *Nlrp2*-null females compared to WT embryos, whereas the transcriptome of heterozygous embryos from *Nlrp2*-null males was not significantly different from that of WT embryos. Maternal absence of NLRP2 also negatively impacted MZT, as evidenced by the deregulation of a large subset of zygotic genome activation (ZGA)-related genes.

Conclusions This study demonstrates that NLRP2 is essential for shaping the transcriptome of GV oocytes and preimplantation embryos. Maternal loss of *Nlrp2* negatively impacts ZGA. Our findings that the DNA methylome of Het and *Nlrp2*-null oocytes was subtly changed, and that gene-body DNA methylation differences did not correlate with gene expression differences, suggest that posttranscriptional changes in transcript stability, rather than altered transcription itself, are primarily responsible for the changed transcriptome of *Nlrp2*-null oocytes.

Keywords Subcortical maternal complex, Oocyte, Imprinted genes, DNA methylation

*Correspondence:
Ignatia B. Van den Veyver
iveyver@bcm.edu
Full list of author information is available at the end of the article

Background

The processes of transcription, translation, mRNA and protein stability and degradation, and epigenetic reprogramming are highly regulated during oogenesis and early embryo development. In mice, previously quiescent oocytes in primordial follicles resume transcription in the early postnatal period, and transcription continues during oocyte growth until it is globally repressed in fully grown germinal-vesicle (GV) stage oocytes [1], but oocytes retain cytoplasmic stores of transcripts and proteins encoded by maternal effect genes (MEGs) that are essential for further oocyte maturation, progression and completion of meiosis, fertilization, and the earliest stages of embryo development. The newly fertilized embryo is also initially transcriptionally quiescent and relies only on maternal products provided by the oocyte. During the maternal-to-zygotic transition (MZT), required for the acquisition of developmental competence by the embryo, maternal products are progressively degraded through a maternal pathway (M-decay) and a zygotic pathway (Z-decay), which requires zygotic genome activation (ZGA) [2, 3]. ZGA is a massive transcription event that occurs in two waves: minor ZGA at the mid-1-cell stage with the activation of a handful of genes through promiscuous transcription and major ZGA at the late 2-cell stage with the activation of thousands of genes. Once ZGA is complete, the embryo begins transcribing its own biparentally inherited genome [4, 5].

In mouse oocytes, transcription drives de novo DNA methylation [6–8]. Approximately 10 days after birth, DNA methylation establishment is initiated by the DNMT3 A/L complex in mouse growing oocytes and is largely completed by the GV stage [9], at around day 21 when oocytes have about 40% global DNA methylation [10–13]. The global DNA methylation landscape of oocytes is unique and differs profoundly from that of somatic cells. In oocytes, which are non-replicative cells, DNA methylation is primarily targeted to actively transcribed units, resulting in a bimodal methylome, consisting of broad hypomethylated domains (HypoDs) and hypermethylated domains (HyperDs). The latter are mostly associated with gene bodies and encompass intragenic CpG islands (CGI) [7, 8, 14]. Other genomic features that acquire methylation in oocytes are maternal germline differentially methylated regions (gDMRs) of imprinted genes [15]. The monoallelic methylation of these gDMRs is necessary for their parent-of-origin monoallelic expression after fertilization and throughout the lifespan [8, 16]. Genetic or epigenetic disturbances in the expression of imprinted genes cause imprinting disorders [17]. Therefore, the necessity for epigenetic marking of gDMRs is an important reason why oocyte DNA methylation is essential for successful development [18].

In mammals, a subset of MEGs code for subcortical maternal complex (SCMC) proteins. The SCMC is a multiprotein complex essential to cytoplasmic lattices (CPLs) of oocytes and cells of preimplantation embryos [19]. This complex plays a vital role in various essential cellular processes during the MZT [20–22]. In mice, NLRP5, TLE6, and OOEP are proteins that constitute the core of the SCMC. KHDC3 integrates into this structure by binding to OOEP. PADI6, NLRP2, and NLRP7 are additional components of the SCMC (the latter only in humans) [23]. NLRP5, OOEP, TLE6, and PADI6 are crucial for development beyond the two-cell stage because their absence from oocytes and embryos before MZT leads to female sterility [24–27], whereas the absence of other SCMC proteins, like NLRP2 and KHDC3, causes milder and variable effects, including delayed preimplantation development and decreased fecundity [28, 29]. Other proteins associated with the complex have since been found, and other components are probably still to be discovered, consistent with estimates of the SCMC's high molecular weight (between 669 and 2000 kDa) [30–35]. A human SCMC has also been identified [36] and maternal loss of function of some of the genes that encode SCMC proteins results in embryonic lethality, biparental complete hydatidiform mole (BiCHM)—a recurring form of hydatidiform mole (HM) characterized by trophoblast overgrowth and the absence of embryo development—and recurrent pregnancy loss [37–41].

Maternal loss of NLRP2 has been associated with a wide array of reproductive and offspring phenotypes in both humans and mice. *Nlrp2* knockdown in mouse GVs causes embryonic arrest between the two-cell and eight-cell stages [32]. We previously showed that female mice lacking *Nlrp2* are subfertile and have adverse reproductive outcomes. Their offspring have variable phenotypes that can include early embryonic loss, growth restriction, delayed development, and congenital anomalies [28]. The embryonic phenotype was exacerbated during in vitro culture, where embryos from *Nlrp2*-null females failed to form blastocysts [42]. We also showed that loss of NLRP2 alters the transcript abundance of hundreds of genes in superovulated metaphase-II (MII) oocytes, potentially contributing to the abnormal reproductive phenotypes and reduced viability of embryos [43]. Although we found abnormal DNA methylation at a few imprinted loci in affected offspring of *Nlrp2*-null females [28], we did not yet examine if the transcriptome changes in MII oocytes were also associated with locus-specific or globally altered DNA methylation. It has also been shown that maternal loss-of-function variants of *NLRP2* in humans cause pregnancy loss and loss of methylation at maternally methylated imprinted gDMRs. This can manifest in a range of imprinting disorders, including multilocus

imprinting disturbance (MLID), transient neonatal diabetes mellitus (TNDM), Beckwith–Wiedemann syndrome (BWS), Silver–Russell syndrome (SRS), as well as signs of growth restrictions and developmental delays in probands that were not consistent with any specific diagnosis [44, 45]. These combined mouse and human data indicate that NLRP2, directly or indirectly, plays a role in epigenetic regulation, supporting a potential broader role for the SCMC in this process. How loss of cytoplasmic NLRP2 and other SCMC proteins impacts epigenetic programming and reprogramming, particularly DNA methylation, remains poorly documented. Our previous work in human showed a genome-wide loss of DNA methylation in oocytes and preimplantation embryos caused by maternal loss of function of *KHDC3L* [46]. Giaccari and colleagues recently found that maternal loss of *Padi6* in mouse oocytes causes genomic hypermethylation, decreased transcript abundance of ZGA genes, and increased transcript abundance of maternal decay genes in 2-cell embryos. In addition, superovulated MII oocytes from *Padi6*-null females had significant transcriptome changes. They also found disrupted intracellular localization of the maintenance DNA methyltransferase 1 (DNMT1), and its cofactor UHRF1 in GV oocytes, zygotes, and 2-cell embryos from superovulated *Padi6*-null females [47].

In the present study, by applying a method of combined profiling of gene expression and DNA methylation, we investigated the molecular changes occurring in *Nlrp2*-null oocytes during early mouse development. We found that gene expression was severely impaired in 2-cell embryos and in GV oocytes at the developmental stage immediately after the completion of oocyte transcription and DNA methylation establishment. Compared to wild-type (WT), the DNA methylation profile of *Nlrp2*-null and *Nlrp2*-heterozygous (Het) GV oocytes exhibited minor changes, which did not correlate with gene expression differences. Collectively, maternal loss of function of *Nlrp2* led to impairments in DNA methylation, gene expression profile, and ZGA in mice.

Results

Absent or reduced *Nlrp2* alters ovarian follicle maturation

We collected GV oocytes from 26- to 28-day-old WT, Het, and *Nlrp2*-null female mice to study their DNA methylome and transcriptome. Oocytes were collected in pools of 60–80 oocytes per animal from both ovaries combined, with each pool from a single mouse serving as one biological replicate (Fig. 1a and Supplementary Fig. 1). To avoid potential reproductive effects of maternally inherited null alleles in Het females, we only included oocytes from Het females who carry a paternally inherited null allele. There was no difference in the number of retrieved oocytes between the three genotypes (one-way ANOVA: $p = 0.66$) (Supplementary Table 1). However, we noted that isolated GVs from *Nlrp2*-null females tended to degenerate faster compared to the other two genotypes, indicating that total absence of NLRP2 reduces oocyte viability. We also counted follicle distribution of both ovaries of five females each per genotype at postnatal day 24 (P24). Compared to WT, *Nlrp2*-null ovaries contained fewer secondary ($p = 0.003$), antral ($p = 0.04$) and ovulatory follicles ($p < 0.001$), but more atretic follicles ($p < 0.001$), and Het ovaries contained fewer antral ($p = 0.016$), ovulatory ($p < 0.001$) but more atretic ($p < 0.001$) follicles (Fig. 1b, c) (multiple comparisons with Bonferroni, Supplementary Table 2). We found by locus-specific qRT-PCR that *Nlrp2* RNA expression was reduced by about 50% in GV oocytes from Het females compared to WT and absent in those of *Nlrp2*-null females (Fig. 1d). Together, these results indicate that the absence or reduction of NLRP2 impairs follicle maturation dynamics.

Genome-wide oocyte-specific DNA methylation patterns are preserved in oocytes from *Nlrp2*-null, Het, and WT mice

We profiled the DNA methylome of seventeen GV oocyte pools, derived from seven WT, five Het, and five *Nlrp2*-null females. We used the post-bisulfite adaptor tagging (PBAT) method with slight modifications [48, 49] to profile genome-wide DNA methylation. After alignment and removal of duplicate sequence reads, we retained between 2,084,314 and 27,718,913 uniquely mapped reads per library for further analysis (Supplementary Table 3). We first observed that the CpG methylation profiles of all PBAT libraries are highly similar, with most of the pairwise correlations greater than 0.8. Moreover, the *Nlrp2*-null libraries and Het libraries cluster closer to each other than to WT libraries (Supplementary Fig. 2A). Sequencing yielded 2,054,114 CpGs as the mean number of CpGs covered by at least 3 reads (3X depth) in each PBAT library (Supplementary Table 3). However, to do a more rigorous analysis we wanted to exclude methylomes from oocyte pools with possible granulosa cell contamination and low read counts. As a proxy for granulosa cell contamination, we used methylation levels at X chromosome CpG islands, which is very low in oocytes, compared to granulosa cells [50], and only included methylomes from pools with an average X chromosome CpG island methylation level of < 13.5%. Additionally, we set up a cutoff for read counts (> 5,000,000 uniquely mapped reads). Applying these exclusion criteria resulted in a total of 11 oocyte methylomes for further analysis: three WT (WT#2, WT#44, and WT#49), four Het (Het#9, Het#10, Het#27, and Het#30), and four *Nlrp2*-null (*Nlrp2*-null#26, *Nlrp2*-null#29, *Nlrp2*-null#33,

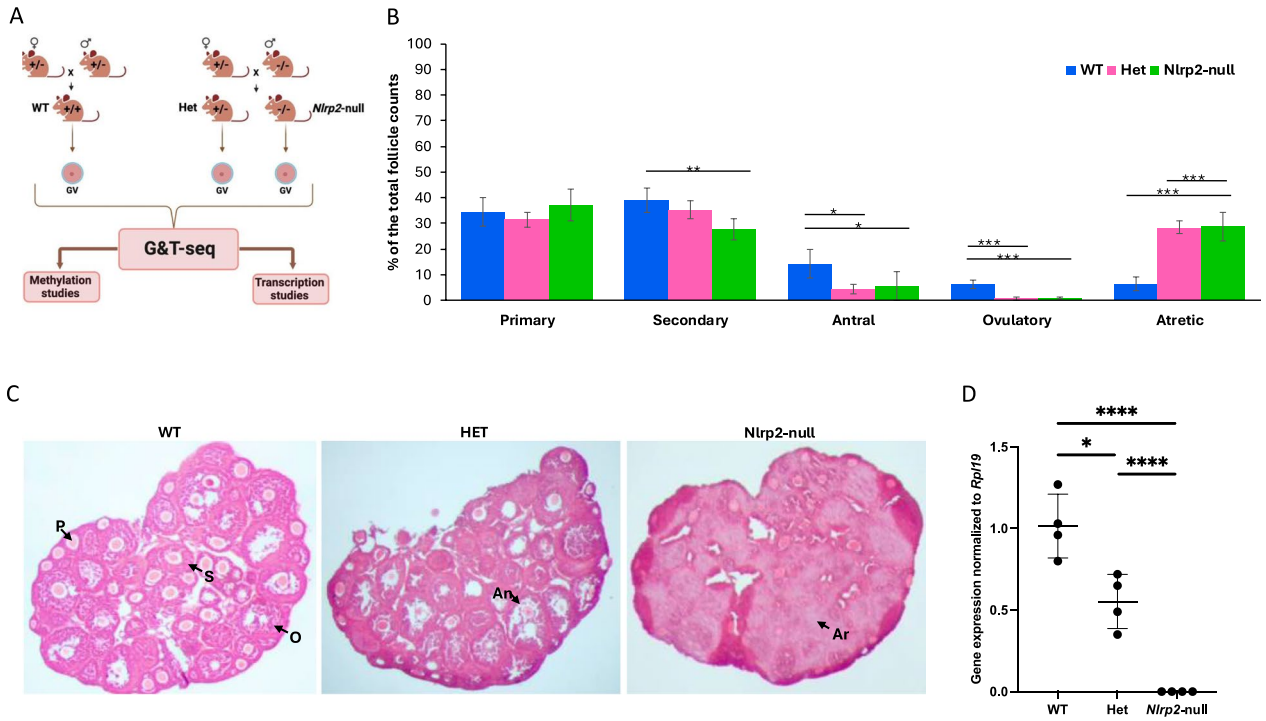

Fig. 1 **a** Experimental design. GV oocytes were isolated from WT, Het, and *Nlrp2*-null females. Each library (biological replicate) was prepared from a pool of 60–80 GV oocytes isolated from both ovaries of one female. **b** Follicle distribution in ovaries from WT, Het, and *Nlrp2*-null mice at P24. We counted five biological replicates of follicles in both ovaries per genotype. Follicle distributions are represented as percentages of total follicular counts (*** = $p < 0.001$, ** = $p < 0.01$, * = $p < 0.05$). **c** Hematoxylin and eosin (H&E) staining of ovarian sections from wild-type (WT), heterozygous (Het), and *Nlrp2*-null mice. Ovaries from Het and *Nlrp2*-null mice exhibit a significant reduction in secondary, antral, and ovulatory follicles compared to WT. Additionally, Het and *Nlrp2*-null ovaries show an increase in atretic follicles relative to WT (P: Primary, S: Secondary, An: Antral, O: Ovulatory, Ar: Atretic). **d** Expression levels of *Nlrp2* in GV oocytes by locus-specific qRT-PCR. Gene expression was normalized to oocyte housekeeping gene *Rpl19*.(* = $p < 0.05$, **** = $p < 0.0001$)

and *Nlrp2*-null#34) (see also supplementary method and Supplementary Fig. 2B–E).

The percentage of genome-wide CpG methylation was 35.1–47.5%, and for non CpG methylation, CHG was 4.1–5.4% and CHH methylation was 4–5.8% across all libraries (Supplementary Table 3). The median CpG methylation was 42.3% in WT oocyte pools, 41.4% in Het oocyte pools, and 42.7% in *Nlrp2*-null oocyte pools, with no statistically significant differences between the genotypes (WT versus Het; T test: $p = 0.63$, WT versus *Nlrp2*-null; T test: $p = 1$) (Fig. 2a).

We also examined DNA methylation levels at all promoters and gene bodies. We found that the median methylation at promoters was significantly lower in Het (1.6%) and *Nlrp2*-null oocytes (2.1%) compared to WT oocytes (3.6%) (Tukey multiple comparisons, $p < 0.001$ for both) (Fig. 2b). Of the 14,089 promoters with desired 3X depth, only 274 had different DNA methylation levels between genotypes (Supplementary Table 4). GO analysis of genes associated with these promoters showed that the most enriched biological processes were mRNA processing (GO: 0006397), blastocyst development (GO: 0001824), and blastocyst hatching (GO: 0001835).

(See figure on next page.)

Fig. 2 **a** Box plot of overall CpG methylation levels for each genotype. The mean CpG methylation levels for each oocyte pool (represented by dots) and the median for each group are indicated. **b, c** Violin plots of methylation levels of promoters (**b**) and gene bodies (**c**). Analysis was performed on 3 WT, 4 Het, and 4 *Nlrp2*-null oocyte pools. **d** Heatmap of methylation levels of maternal and paternal gDMRs in 3 WT, 4 Het, and 4 *Nlrp2*-null oocyte pools (0–100 represents % methylation). **e** Methylation levels of oocyte-specific CGIs in WT, Het, and *Nlrp2*-null oocyte pools. Box plots show median (center line), upper and lower quartiles (box limits), 1.5X interquartile range (whiskers), and outliers (points). **f** Violin plot of genome-wide DNA methylation in 100-CpG tiles on selected pools of 3 WT, 4 Het, and 4 *Nlrp2*-null oocytes. These libraries exhibit the expected highly bimodal pattern, but with more variability in Het and *Nlrp2*-null oocyte pools

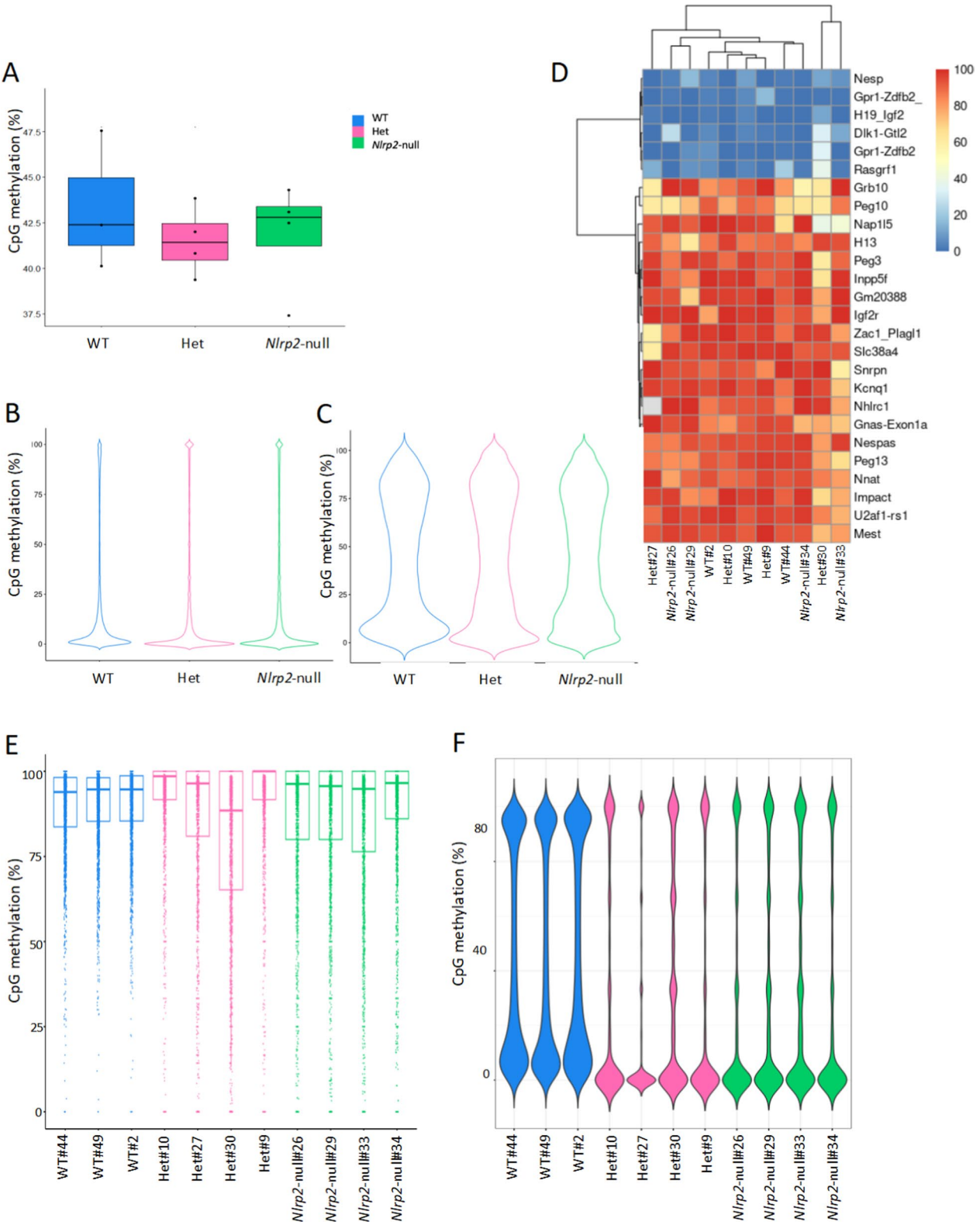

Fig. 2 (See legend on previous page.)

When we quantified methylation levels over gene bodies, we saw no differences between *Nlrp2*-null (41.9%) and WT (41.8%) oocytes, but slightly higher methylation in Het oocytes (43.5%) compared to WT oocytes (Tukey test for multiple comparisons, $p = 0.003$) (Fig. 2c).

We next sought to comprehensively investigate the properties of various characteristic CpG methylation features of oocytes, including the methylation patterns and levels of gDMRs, CpG islands (CGIs), oocyte-specific CGIs, and the presence of a bimodal DNA methylome, which can serve as indicators of fidelity of oocyte CpG methylation pattern.

We evaluated CpG methylation levels of gDMRs because of their importance in early development and genomic imprinting. We found that maternal gDMRs are highly methylated and paternal gDMRs are unmethylated in oocyte pools, with no difference between the three genotypes (Fig. 2d). Then, we investigated the methylation levels of CGIs in the oocyte pools. We had sufficient coverage to analyze DNA methylation of a subset of 11,720 CGIs of the total ~23,000 present in the mouse genome [8, 51]. Applying a threshold of $q < 0.05$ and methylation difference of 10%, we found that only six CGIs had differential methylation between WT and Het oocytes and only nine between WT and *Nlrp2*-null oocytes (Supplementary Table 5). We then assessed CpG methylation levels at the 2,140 highly methylated oocyte-specific CGIs [8, 51] as an additional indicator of the expected methylation pattern of normal oocytes and found that all were highly methylated, irrespective of oocyte genotypes (Fig. 2e). Hence, even though Het and *Nlrp2*-null oocytes had more variable overall methylation patterns compared to WT oocytes, methylation at gDMRs and CGIs was not significantly impacted by reduced or absent NLRP2. This is not unexpected given the nature of these genomic elements, as any impact on their methylation is expected to cause a pronounced embryonic phenotype, which is inconsistent with outcomes in embryos conceived from *Nlrp2*-null females [28].

Next, to ascertain the bimodal DNA methylome of mouse oocytes, we employed an unbiased 100-CpG tiling approach, with each tile containing 100 consecutive CpGs. As shown in Fig. 2f, the analyzed 11 methylomes exhibit the expected bimodal DNA methylation pattern of oocytes, with the lower bump on the violin plot corresponding to regions with low methylation levels (perhaps HypoDs), and the upper bump corresponding to regions with high methylation levels (perhaps HyperDs). These results indicate similar global DNA methylation landscapes in oocytes of the three genotypes.

Distinct changes in DNA methylation at discrete loci in GV oocytes lacking *Nlrp2*

The above quantitative analysis of 100-CpG tiles (Fig. 2f) indicates that the bimodal DNA methylation pattern representative of the presence of HyperDs/HypoDs is consistently observed in all 11 tested oocyte methylomes. However, this does not provide details on the number, distribution, and actual methylation levels of HyperDs/HypoDs. To address this, we examined the methylation levels of each individual HyperD or HypoD. We retained 71,941 HyperDs/HypoDs in our WT oocyte methylomes (out of originally reported 94,513 by Veselovska and colleagues [7]). The methylation levels of each of these domains were then measured (Fig. 3a). This analysis showed that all oocyte pools—irrespective of their genotypes—contain characteristic oocyte-specific HyperDs and HypoDs (Fig. 3a). To further confirm the specificity of this analysis, we also aligned methylation profiles from granulosa cells (which are not expected to be enriched for HyperDs and HypoDs) and confirmed the absence of HyperDs and HypoDs in those cells (left three lanes in Fig. 3a). (See also supplementary method and Supplementary Fig. 2B–E). To further examine the distribution of HyperDs/HypoDs, assess whether specific location of HyperDs/HypoDs is maintained or lost, and if new ones emerged in Het and *Nlrp2*-null oocytes, we set up a cutoff for HyperDs as average methylation $\geq$ 75% and for HypoDs as average methylation of $\leq$ 25%. We found that of the known HyperDs and HypoDs, 63,189 domains (27,800 hyper and 35,389 hypo) were collectively maintained in both the Het and the *Nlrp2*-null oocytes (Fig. 3b common between the both blue donut graphs). We also found that 835 HyperDs and 781 HypoDs did not reach these thresholds in Het oocytes (Fig. 3b left) and that 1,172 HyperDs and 1,239 HypoDs did not reach these thresholds in *Nlrp2*-null oocytes (Fig. 3b right), which we interpreted those as lost HyperDs and HypoDs. This indicates that even though only a small fraction of HyperDs and HypoDs are lost from Het and *Nlrp2*-null oocytes, the overall structure and distribution of HyperDs and HypoDs—a signature feature of oocytes—are sensitive to maternal loss and haploinsufficiency of NLRP2.

We next sought to identify any generally differentially methylated regions (DMR) between Het and WT oocytes and between *Nlrp2*-null and WT oocytes. For this analysis, we employed the adjacent 10-kb tiling approach, which yielded 252,972 informative tiles with 3X depth in all 11 samples. A methylation difference of a tile was considered statistically significant by a chi-square test corrected for multiple comparisons using the SLIM method ($q < 0.01$) and when the difference between two genotypes was $\geq$ 20%. Applying these criteria, we identified 378 hypomethylated and 599 hypermethylated DMRs in

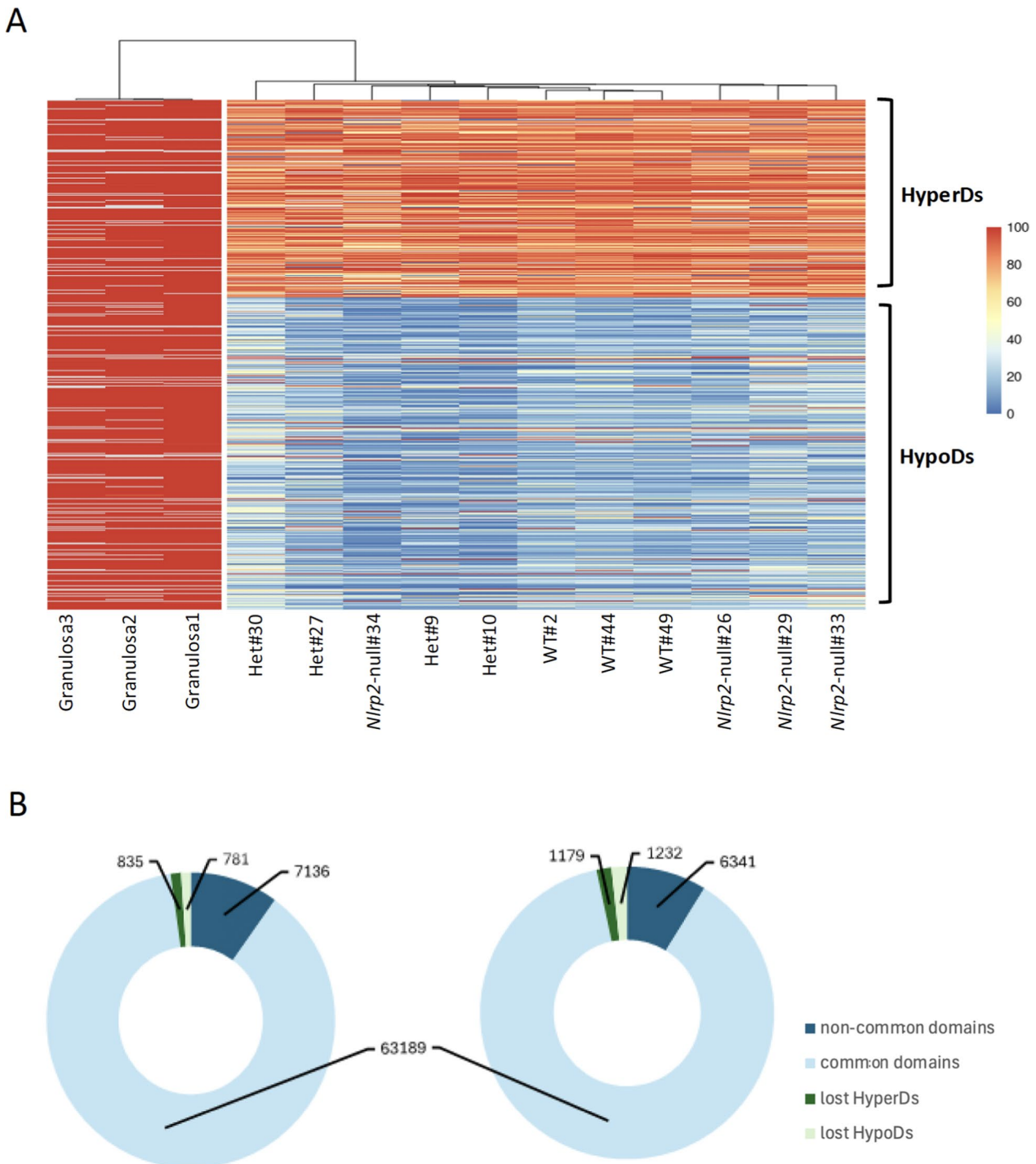

Fig. 3 **a** Heatmap of distribution of HyperDs and HypoDs: HyperDs (upper cluster) and HypoDs (lower cluster) of selected oocyte pools (right 11 lanes) compared to granulosa cells (three left lanes) are shown. (0–100 scale represents relative methylation levels.) **b** Doughnut graphs of maintained and lost HyperDs and HypoDs in Het and *Nlrp2*-null oocyte pools. Each donut represents the 71,941 analyzed domains in this comparison. Colors and numbers indicate maintained domains (sum of dark and light blue), lost HyperDs (dark green), and lost HypoDs (light green) in Het (left) and *Nlrp2*-null (right) oocytes

Het compared to WT oocyte pools (Fig. 4a) (Supplementary Table 6) and 907 hypomethylated and 1393 hypermethylated DMRs in *Nlrp2*-null oocytes compared to WT oocytes (Fig. 4b, c) (Supplementary Table 7). These DMRs were evenly distributed across all chromosomes (Fig. 4c), but we noted that *Nlrp2*-null and Het DMRs were more abundant in intergenic regions than in promoters, exons, or introns (one-way ANOVA, $p = 0.01$) (Supplementary Fig. 3). There were 87 DMRs in common between Het versus WT and *Nlrp2*-null versus WT comparisons, which were equally distributed across chromosomes (Fig. 4c, d). Although a gene may be much larger than a DMR, which spans a 10 kb tile, we have identified interesting genes or clusters associated with these common DMRs. The first is the maternally imprinted *Gnas* gene, residing in a locus with a highly complex imprinted expression pattern. The second gene is *Jarid2,* encoding a cofactor of polycomb complex PRC2, which methylates histone mark H3 K27 and is essential for embryonic stem cell differentiation and preimplantation development [52]. The third are the *Obox1* and *Obox3* genes, which are required for oocyte maturation, ZGA, and early embryogenesis [53]. These methylation changes, which are more pronounced in *Nlrp2*-null oocytes, underscore the importance of profiling the transcriptome.

Maternal loss of *Nlrp2* alters the transcriptome of GV oocytes

We next profiled the transcriptome of twelve GV oocyte pools, derived from seven WT and five *Nlrp2*-null females. Upon running the standard analysis pipelines, we observed some overexpressed unannotated genes that appeared as novel splices between genes that share a high degree of similarity. These could result from the presence of variable amounts of unprocessed RNA, DNA contamination in the cDNA libraries or library over-amplification. To ensure a rigorous analysis, we excluded the approximately 10% of reads associated with these splices and retained only those aligning entirely across known splice junctions. The detailed metrics of the RNA sequencing (RNA-seq) experiments are in Supplementary Table 8. An Euclidean distance-based correlation matrix of gene counts showed a correlation between samples (Fig. 5a) and principal component analysis indicated a clear separation of oocyte transcriptomes by genotype (Fig. 5b). After selecting only those genes that were covered by at least one read in at least one sample, we retained 15,487 genes, with an average of 13,022 per library. Of these, 10,861 were in common between all libraries. Of note, fewer expressed genes were detected in *Nlrp2*-null oocytes compared to WT oocyte (Fig. 5c) (Wilcoxon test: $p = 0.03$), which indicates a shift in oocyte maturation. This coupled with impaired follicle maturation suggests that the overall reproductive maturation in these animals is delayed.

Differential gene expression was determined by DESeq2 analysis on the combined oocyte pools from each genotype followed by filtering for genes with |Log2 FC|> 1 and adjusted p value < 0.05. It is important to recognize for this analysis that fully mature GV oocytes at the surrounded nucleolus (SN) stage are transcriptionally quiescent cells that store previously transcribed RNAs. Therefore, the identification of differentially expressed genes (DEGs) is not solely indicative of differences in transcriptional activity between genotypes but could also reflect altered RNA abundance that arose from differences in posttranscriptional processes that influence RNA stability and degradation. Thus, for this analysis the term "overexpressed DEGs" refers to more abundant transcripts, while "underexpressed DEGs" refers to less abundant transcripts. We found 858 DEGs between *Nlrp2*-null and WT oocyte pools (Supplementary Table 9). Of these, 418 were overexpressed and 440 were underexpressed in *Nlrp2*-null oocytes (Fig. 6a and Supplementary Fig. 4A). Strikingly, the overexpressed DEGs contain many genes that encode important epigenetic regulators, including ZFP57, DNMT1, UHRF1, and KDM1B, and genes that encode other proteins of the SCMC, including TLE6, ZBED3, and PADI6. This highlights the involvement of NLRP2 in early development through these factors.

We validated the accuracy of our RNA-seq data by locus-specific qRT-PCR. Supplementary Fig. 4B reports the significant difference between RNA expression between WT and *Nlrp2*-null of 3 different genes *Nlrp2*,

(See figure on next page.)

Fig. 4 Scatterplots of average methylation values of 10 Kb tiles: **(a)** Comparison between Het ($n = 4$) and WT oocyte pools ($n = 3$), and **(b)** *Nlrp2*-null ($n = 4$) and WT oocyte pools ($n = 3$). Each dot is one tile. Red is hypermethylated in Het or *Nlrp2*-null and blue is hypomethylated in Het or *Nlrp2*-null compared to WT oocytes. **c** Circos graph comparing genome-wide methylation levels in *Nlrp2*-null versus WT and Het versus WT oocytes by chromosome. From outer to inner circle: Chromosomes number and size, G-banding pattern, 87 common DMRs, all informative tiles in *Nlrp2*-null versus WT in light blue, a brush indicating occupancy of DMRs out of all informative tiles in black, the 2300 DMRs identified in *Nlrp2*-null versus WT in brown to green, a brush indicating the occupancy of DMRs out of all informative tiles in black, the 977 DMRs identified in Het versus WT in brown to green, all informative tiles in Het versus WT in light blue (Brown to green represents low to high methylation differences). **d** Venn diagram of the number of unique and common DMRs between *Nlrp2*-null versus WT (green) and Het versus WT (pink) comparison

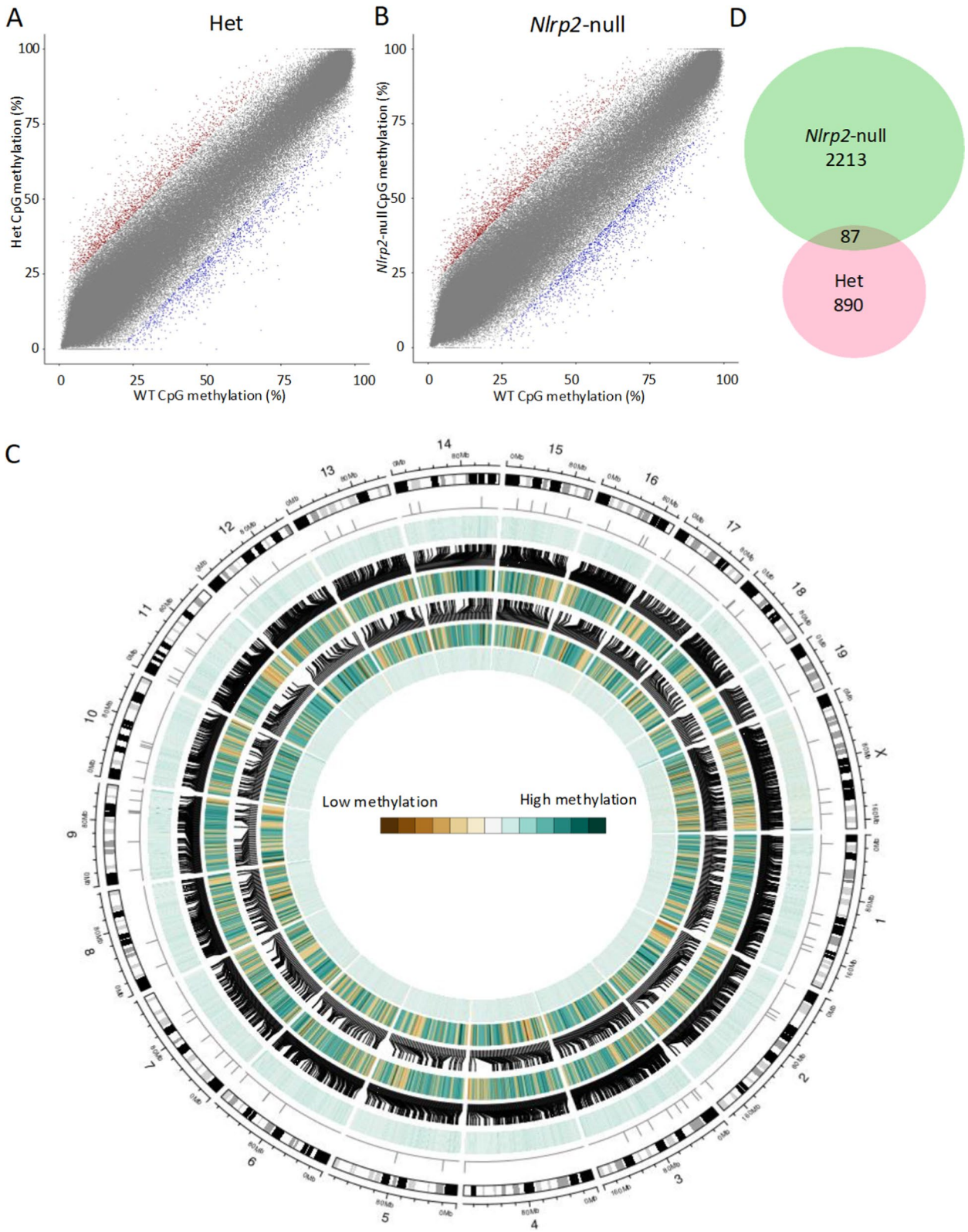

Fig. 4 (See legend on previous page.)

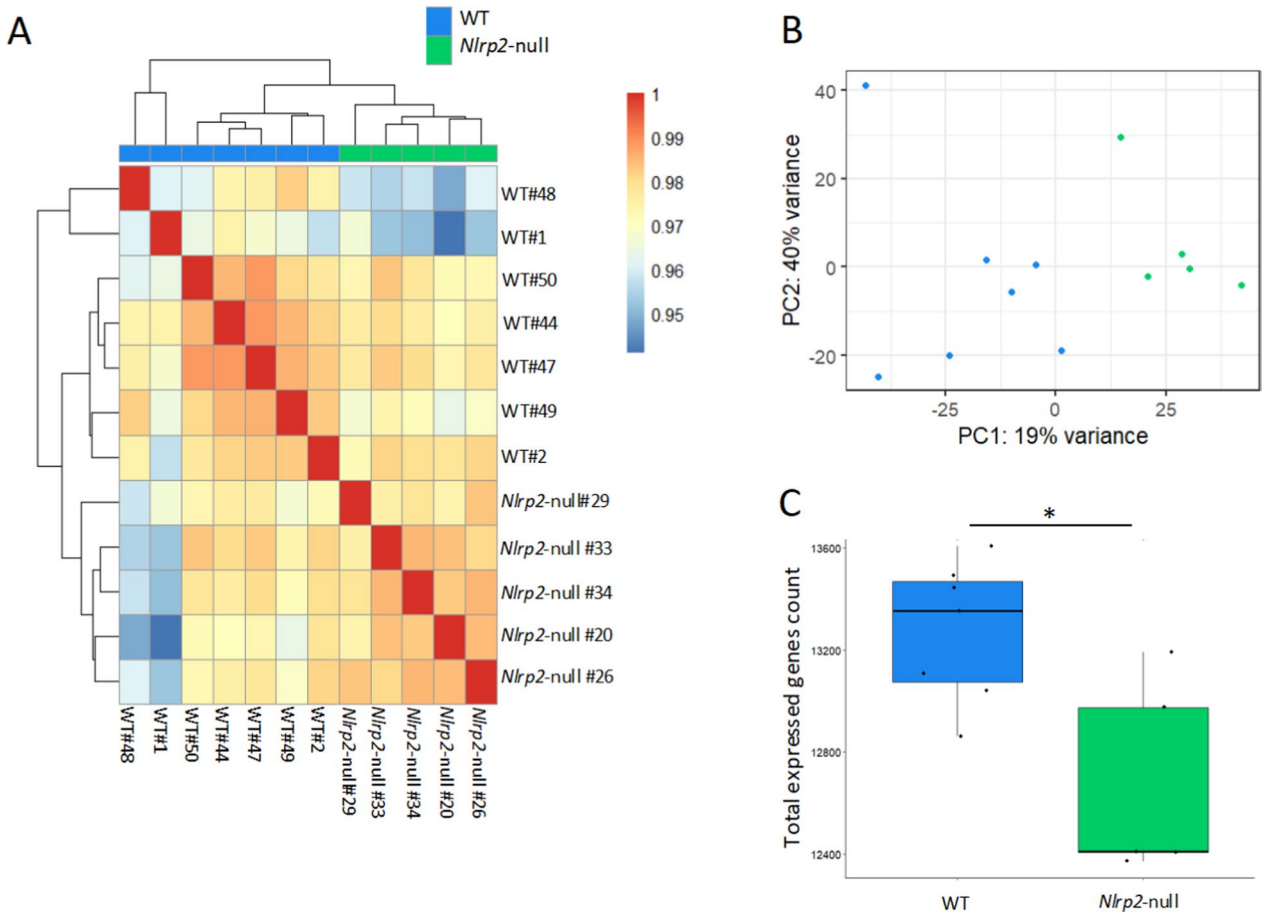

Fig. 5 **a** Correlation matrix for GV oocyte RNA-seq libraries. This heatmap shows the pairwise Euclidean distances between RNA-seq libraries after applying a variance stabilizing transformation (VST) to the gene count data. Each cell corresponds to the calculated distance between two RNA-seq libraries, providing a visual representation of library similarity, where a value of 1 is an ideal correlation. **b** PCA Plot of Genotype Clustering. Dots in the plot represent an RNA-seq library colored by genotype (WT: blue, *Nlrp2*-null: green). The two genotypes exhibit clear separation along the principal components. X-axis: Principal Component (PC) 1 and Y-axis: PC2. **c** Box plot showing total number of expressed genes in oocytes from WT and *Nlrp2*-null. The mean number of expressed genes for each library (represented by dots) and the median for each group are indicated (*$=p<0.05$)

Trim28, and *Obox3*, which supports the reliability of our transcriptome data.

We then conducted Gene Ontology (GO) enrichment analysis to find the most enriched biological processes among the identified DEGs. Overexpressed DEGs were enriched for regulation of gene expression (GO:0010468), prevention of polyspermy (GO:0060468), embryo development (GO:0009790), and nervous system development (GO:0007399). Underexpressed DEGs were enriched for aerobic respiration (GO:0009060), gamete generation (GO:0007276), mitochondrion organization (GO:0007005), RNA processing (GO:0006396), and apoptotic process (0006915). All these biological processes align with the recognized role of the SCMC in early development.

We next inspected MA plots which visualize DEGs between *Nlrp2*-null and WT oocytes (Fig. 6b) while also factoring in the average overall expression levels for each gene across both genotypes. We found that DEGs in the *Nlrp2*-null to WT comparison are distributed across the entire range of expression levels (Fig. 6b). However, we noted that highly abundant genes are enriched for overexpressed DEGs and lowly abundant genes are enriched for underexpressed DEGs. This observation, coupled with the identification of lower overall expressed gene counts in oocytes of *Nlrp2*-null mice, along with the impaired follicle maturation in those mice, implies that *Nlrp2*-null oocytes are distinctly different from WT oocytes.

No correlation between GV oocyte DNA methylation and transcription

Given that transcription drives DNA methylation establishment within gene bodies in oocytes, we aimed to explore the relationship between gene expression and

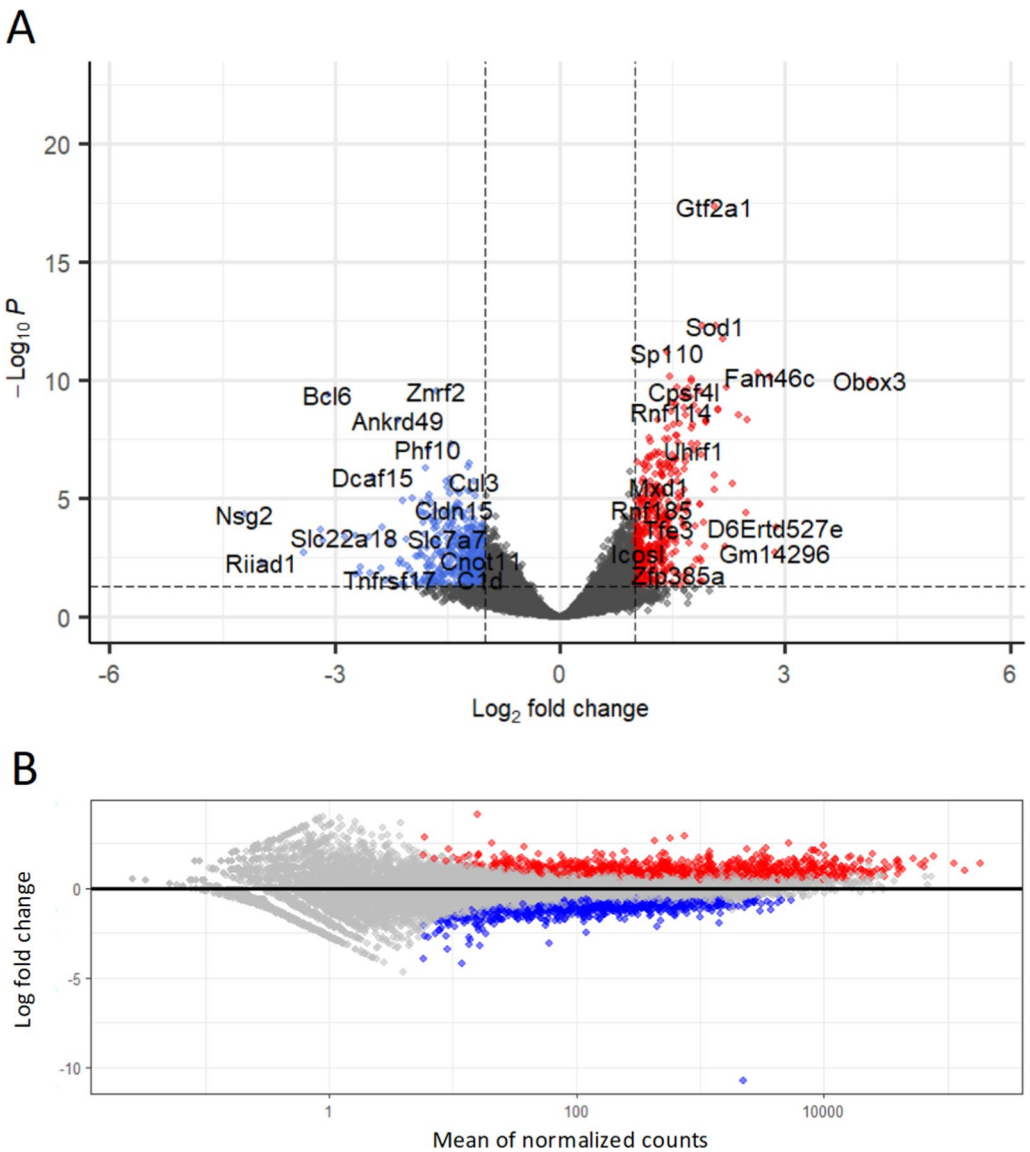

Fig. 6 **a** Volcano plot of DEGs between *Nlrp2*-null and WT oocyte pools. Note: we removed *Nlrp2* for better visualization of the other DEGs but refer to Supplementary Fig. 5A for volcano plot that includes *Nlrp2* (Red: overexpressed genes; blue: underexpressed genes; gray: genes without significant expression difference; vertical dashed lines: Log2 FC cutoff; horizontal dashed lines: significance level). **b** MA plots of Log2 fold changes (y-axis) over mean expression levels (x-axis) in *Nlrp2*-null versus WT oocyte pools (with same colors for DEGs)

DNA methylation using integrative scatter plots that contrast the expression differences of DEGs with their corresponding gene-body DNA methylation differences. We analyzed the 230 DEGs from the *Nlrp2*-null versus WT comparison that also had available methylation data (Supplementary Table 10). There was no correlation for *Nlrp2*-null to WT comparison (Spearman correlation coefficient of 0.056, $p = 0.4$; Supplementary Fig. 5A). To further investigate the correlation between gene expression and DNA methylation, we selected the top 25% of DEGs and plotted them against the top 25% of genes with the highest gene-body methylation differences (Supplementary Fig. 5B). This analysis yielded 19 DEGs (Supplementary Table 10) containing intriguing targets for potential future detailed analysis including *Uhrf1*, encoding a DNMT1 cofactor, and *Obox3*, which is required for oocyte maturation, ZGA and early embryogenesis [53].

The absence of a strong correlation between gene expression and DNA methylation differences suggests that the methylation differences between *Nlrp2*-null and WT oocytes are likely not driven by altered transcription. This may be because identified DEGs predominantly

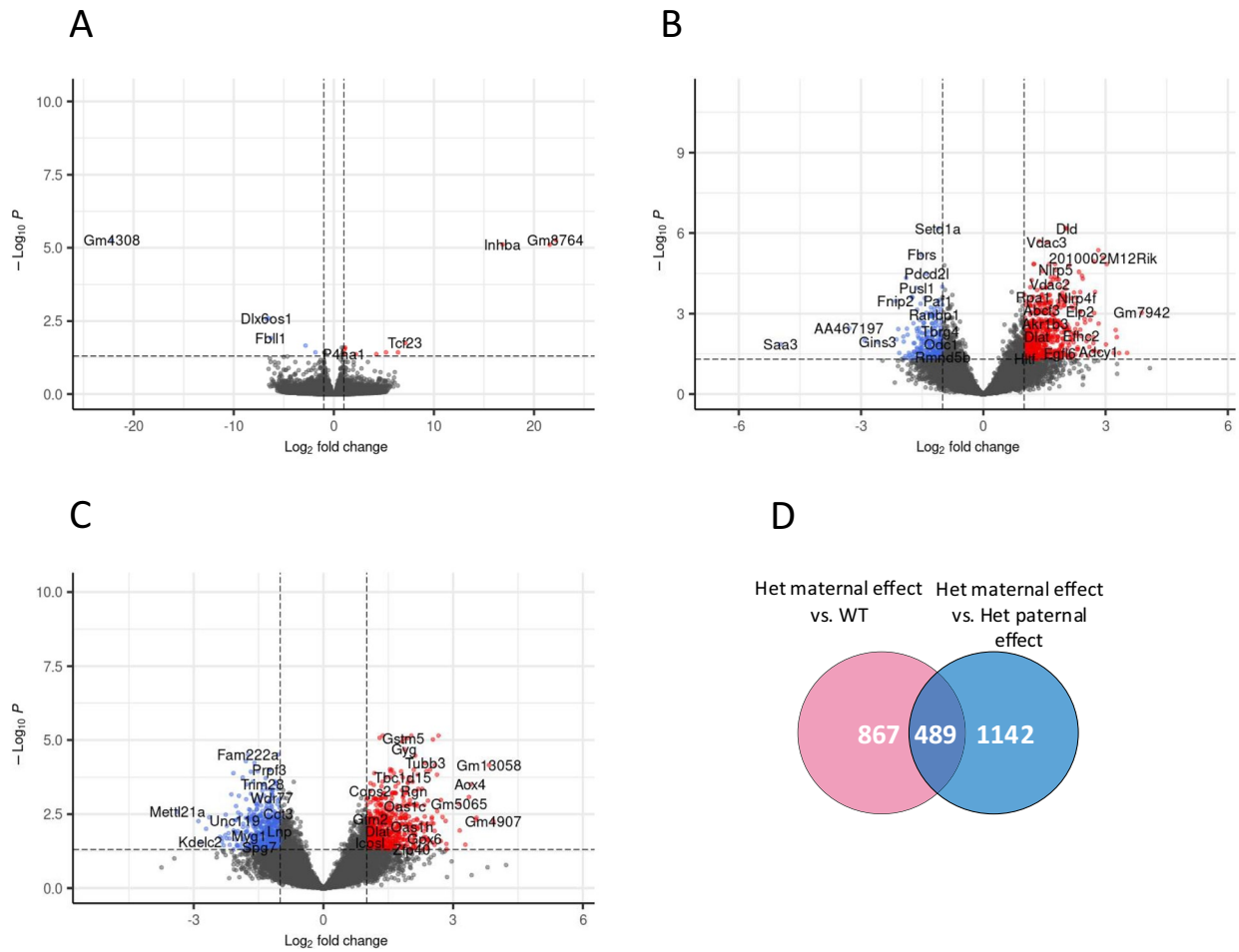

Fig. 7 Volcano plots of DEGs between Het paternal effect and WT embryo pools (**a**), DEGs between Het maternal effect and WT embryo pools (**b**), and DEGs between Het maternal and Het paternal effect embryos (**c**). Red: overexpressed genes; blue: underexpressed genes; gray: genes without significant expression difference; vertical dashed lines: Log2 FC cutoff; horizontal dashed lines: significance level. **d** Venn diagram of the number of unique and common DEGs between Het maternal effect versus WT and Het maternal effect versus Het paternal effect comparisons

result from posttranscriptional changes in transcript abundance from altered RNA stability and RNA degradation, rather than from changes in active transcription.

Maternal loss of *Nlrp2* alters the transcriptome of embryos and negatively impacts maternal-to-zygotic transition

We profiled the transcriptome of 11 WT, 10 Het paternal effect, and 10 Het maternal effect single late 2-cell-stage embryos. Embryos were isolated at embryonic day 1.5 (E1.5) from the matings mentioned in Supplementary Fig. 6A. There was no statistically significant difference in the number of embryos retrieved from each genotype (Supplementary Fig. 6B) and no morphological differences among embryos of the three genotypes (Supplementary Fig. 6C).

Detailed metrics for the RNA-seq experiments are provided in Supplementary Table 11. Each RNA-seq library had an average read count aligned to genes of 14,794,747 (range 11,644,940—20,093,305). After filtering for genes covered by at least one read in at least one sample, we retained an average of 18,123 genes (with no statistically significant difference between genotypes), which were taken into consideration for further analysis.

We identified 17 DEGs between Het paternal effect and WT embryo pools, 867 DEGs between Het maternal effect and WT embryo pools, and 1,142 DEGs between Het maternal and Het paternal effect embryos (Supplementary Table 12). Of the 17 DEGs between Het paternal effect and WT embryos, 11 were overexpressed and 6 were underexpressed in Het paternal effect embryos. Among the 867 DEGs between Het maternal effect and WT embryos, 614 were overexpressed and 253 were underexpressed in Het maternal effect embryos. Of the 1,142 DEGs between Het maternal and Het paternal

effect embryos, 652 were overexpressed and 490 were underexpressed in Het maternal compared to Het paternal effect embryos (Fig. 7a–c). Interestingly, key regulators of mouse ZGA including genes in the *Zscan* family, the *Tcstv* family, the *Obox* family, and *Trim43* were deregulated with maternal absence of NLRP2.

There are 489 DEGs in common between Het maternal effect versus WT and Het maternal effect versus Het paternal effect comparisons (Fig. 7d) (Supplementary Table 12). Of these, 129 were underexpressed and 360 DEGs were overexpressed in both comparisons. Notably, genes encoding important epigenetic regulators such as *Zfp57* and other genes encoding for SCMC proteins, including *Nlrp5*, *Ooep*, *Nlrp9*, and *Nlrp4 F*, were among the commonly overexpressed DEGs. The most enriched biological processes among the commonly overexpressed DEGs include DNA damage response (GO: 0006974), regulation of defense response (GO: 0031347), regulation of programmed cell death (GO: 0043067), and regulation of transcription by RNA polymerase II (GO: 0006357).

To investigate how the identified DEGs in Het maternal effect embryos relate to genes that are altered during MZT, we compared the transcriptome data from GV oocytes of WT females with WT 2-cell embryo data (Fig. 8 middle panel). There were 8,819 DEGs (5,064 overexpressed and 3,755 underexpressed) between WT GV oocytes and WT 2-cell embryos. These represent genes whose expression or abundance changes during the transition from the GV state to the early embryonic state in WT and are thus used as the reference set (Supplementary Table 13). We next investigated if a subset of the overexpressed DEGs in the WT GV to embryo transition are directly involved in ZGA and found that 50% of a published list of major ZGA genes [54] were among the 5064 overexpressed DEGs. Similarly, we checked if a subset of the underexpressed DEGs between WT GV and embryos are among the maternal pathway (M-decay) genes and again found that 48% of the published M-decay genes were among the 3,755 underexpressed DEGs in this reference list.

We then compared the identified DEGs in Het maternal effect 2-cell embryos versus WT 2-cell embryos with the above 8,819-gene reference list (Fig. 8 left panel). This yielded 598 common DEGs, with 207 underexpressed and 391 overexpressed in the Het maternal effect compared to the reference list (Supplementary Table 14). Interestingly, 73% of these 207 underexpressed genes in the Het maternal effect embryos follow an opposite trend in the reference list, indicating that genes expected to be overexpressed during the transition from the GV to 2-cell embryo were underexpressed as a result of maternal absence of NLRP2. Additionally, 95% of the 391 overexpressed genes in Het maternal effect follow the opposite trend in the reference list, suggesting that genes normally

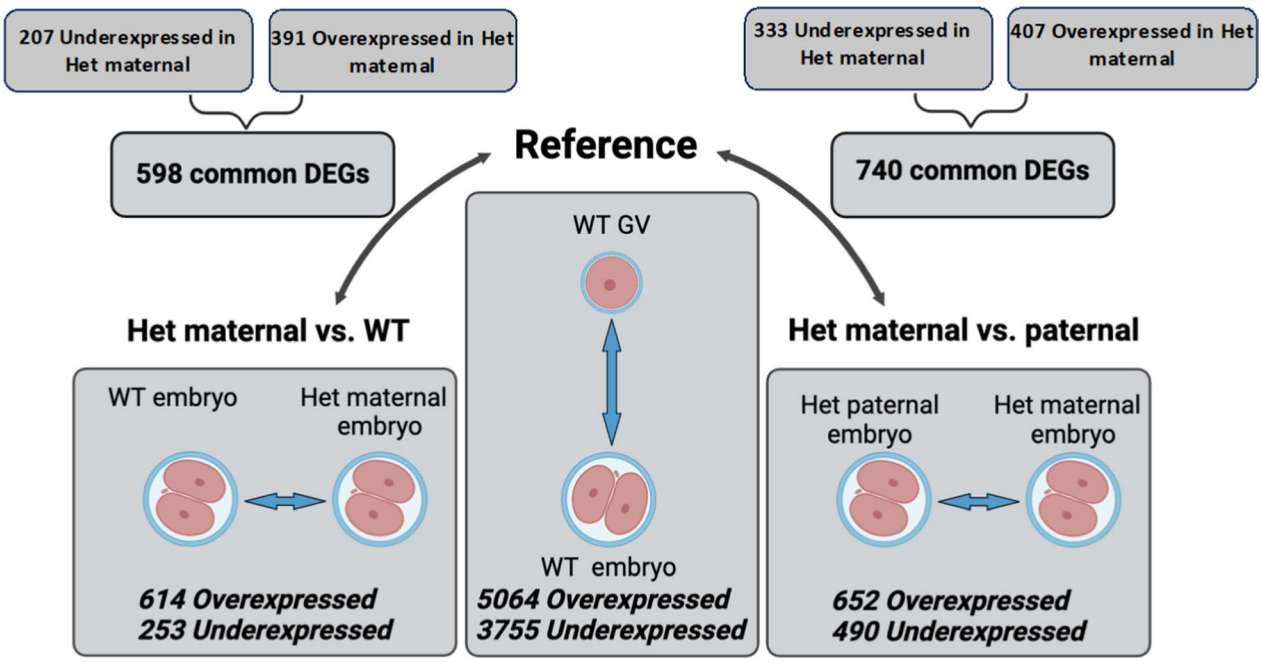

Fig. 8 Schematic showing the strategy to investigate the role of DEGs during MZT. The reference list was obtained by comparing RNA-seq data from WT GV oocytes and WT 2-cell embryos (middle panel). Left and right panels represent the DEGs identified in Het maternal effect versus WT embryos and in Het maternal effect versus Het paternal effect embryos, respectively. Curved arrows on the left and right represent the comparison between these lists of DEGs and the reference list

silenced during the transition from GV to 2-cell embryo were instead overexpressed with maternal absence of NLRP2. Genes that code for many important epigenetic regulators including ZFP57, KDM1B, SETD1 A and for other SCMC proteins, including NLRP5, NLRP14, NLRP9abc, PADI6, TLE6, and OOEP, were among the DEGs that exhibited opposite expression patterns.

Additionally, we compared the identified DEGs between Het maternal effect embryos versus Het paternal effect embryos with genes of the reference list (Fig. 8 right panel). This yielded 740 common DEGs, with 333 underexpressed in Het maternal effect and 407 overexpressed in Het maternal effect embryos (Supplementary Table 15). Again, 81% of the 333 underexpressed genes in the Het maternal and 83% of the 407 overexpressed genes in the Het maternal effect embryos exhibit an opposite trend compared to the reference list. This corroborates the expectation that the transcriptome of Het paternal effect embryos closely resembles that of WT embryos, indirectly suggesting that Het paternal effect embryos are similar to WT embryos.

Finally, we overlapped the 598 genes from the reference list that were differentially expressed in Het maternal effect embryos compared WT embryos with published minor ZGA and major ZGA gene lists [54]. We found that of the 207 overexpressed DEGs, only 17 (8%) overlapped with the minor ZGA published list, but as many as 99 (48%) overlapped with the major ZGA gene list. Additionally, 279 (71%s) of the 391 underexpressed DEGs overlapped with the published M-decay gene list. Taken together these results demonstrate that the absence of maternal NLRP2 impaired ZGA in 2-cell embryos.

Discussion

NLRP2 is a protein of the SCMC of oocytes and preimplantation embryos. Maternal NLRP2 function in oocytes is important for methylation and expression of imprinted genes in placentas and embryos or offspring in both humans and mice [28, 55–57]. Our previous studies in *Nlrp2*-null mice have shown that maternal complete loss of NLRP2 causes reduced fecundity, embryonic and placental defects, and offspring with birth defects and growth abnormalities, with evidence of methylation and expression changes at selected imprinted loci. These defects cannot be rescued by embryo transfer into the uterus of WT females [42], implying that they originate in oocytes. This is further supported by our observation that ovaries of *Nlrp2*-null females have altered follicle distribution [28], itself a feature that had not been previously reported for inactivation of other similar SCMC protein coding genes, such as TLE6, KHDC3, and NLRP5, but investigations of oocyte and follicle morphology in those reports were more limited [25, 26, 29]. This supports that NLRP2 has a broader role in epigenetic reprogramming during early development, with important consequences for pregnancy and offspring development. Although altered oocyte and early embryo epigenetic reprogramming has been shown in mouse oocytes and embryos lacking another SCMC protein, NLRP14 [58], this has not yet been examined for NLRP2. Although the reproductive phenotypes of maternal loss of NLRP2 are variable, there are currently no studies that have examined if these phenotypes are only observed with complete loss of maternally expressed SCMC proteins like NLRP2, or whether their dosage is important.

To this end, we characterized how loss of NLRP2 in oocytes and 2-cell embryos impacts their development, transcriptome, and methylome. We performed, to our knowledge, the first detailed morphological characterization of ovarian follicles of *Nlrp2*-null, *Nlrp2*-Het, and WT females, followed by parallel transcriptome and methylome profiling using the G&T-seq protocol on isolated GV-stage oocytes from 26- to 28-day-old female mice. Confirming our previous data [28], we found altered follicle distribution in the ovaries of *Nlrp2*-null mice, with fewer secondary, antral and ovulatory follicles and more atretic follicles, and we also noted that GV oocytes from *Nlrp2*-null mice tend to degenerate faster during isolation. Both observations indicate that the GV oocytes from the *Nlrp2*-null mice are developmentally compromised, even though all current data indicate that they are fertilization-competent in both human and mice, although with variable embryo development and pregnancy outcomes. We found that ovaries from Het females also have altered follicle distribution, with fewer antral and ovulatory follicles and more atretic follicles compared to WT. This was unexpected since these mice are fertile and have no known adverse reproductive outcomes [28], but is the first indication that not only loss, but also reduced NLRP2 dosage negatively impacts oocyte development. The reduction in antral and ovulatory follicles in Het mice, despite their fertility, suggests that NLRP2 plays a critical role in follicle maturation and that even partial loss of function can disrupt this process. While Het mice are fertile, the reduction in follicles may not necessarily translate to a reduction in the number of ovulated oocytes but could instead affect the quality of the oocytes. To our knowledge, this has not been reported for any other mouse model with inactivation of genes encoding proteins of the SCMC. Interestingly, this observation may be relevant to data from some human studies showing that heterozygous maternal loss of NLRP2 and other SCMC proteins is associated with early pregnancy loss and other adverse reproductive outcomes [40, 45, 59–61].

This prompted us to perform comprehensive epigenetic profiling of GV oocytes and 2-cell embryos. We selected the GV oocyte stage because it is the closest to the time that transcription and methylation establishment in oocytes is complete, making it less likely that any observed changes result from altered oocyte growth or maturation beyond this stage. Furthermore, this preovulatory stage also allowed us to collect enough oocytes from ovaries without needing superovulation, which is required for collecting larger numbers of post-ovulatory oocytes. This is important because superovulation recruits oocytes that are not primed for ovulation and therefore may not have completed epigenetic maturation, and effects of superovulation on oocyte gene expression have been demonstrated in some studies [62]. Another reason we wanted to avoid superovulation is because it has been reported that hormonal treatments used in superovulation protocols can reduce DNMT1 protein expression in mouse GV oocytes [62]. Moreover, our previous study showed that superovulation of *Nlrp2*-null female mice results in more severe embryo phenotypes [28]. We found that GV oocytes of null females have altered transcript abundance and methylation patterns compared to WT oocytes. This indicates that there is a mismatch between the significant morphological and molecular phenotypes of GV oocytes and the reproductive outcomes, since oocytes of both *Nlrp2*-null and Het mice are fertilization-competent, with fertilized Het oocytes, yielding pregnancies with comparable outcomes to WT.

There were several interesting findings in the methylation profile data. *First*, genome-wide DNA methylation levels of Het and Null oocytes were not significantly different from those of WT oocytes. *Second*, when we examined imprinted gDMRs, we confirmed high methylation of maternal gDMRs and low methylation of paternal gDMRs, with no difference between genotypes. Similarly, only very few CGIs (~ 0.1%) and none of the oocyte-specific CGIs had different methylation between genotypes. These observations are consistent with those in oocytes of *Padi6* and *Nlrp14* knockout mouse models [47, 58]. The few genes under control of CGIs that had altered methylation include *Fzd5* (essential for yolk sac and placental angiogenesis [63]), *Hfm1* (mutations of which are linked to decreased embryo development capacity and increased number of cell division times [64]), *Parp8* (required for spindle positioning to oocyte cortex and mediating asymmetric divisions [65]), *Fgfr2* (crucial for trophectoderm development and blastocyst implantation [66]), and *Tcf3* (required for proper axial mesoderm structures in the early embryo [67]). *Third*, when we examined the larger hyper- and hypomethylated domains (HyperDs and HypoDs) characteristic of oocytes, we found that quantitatively, the overall bimodal methylation patterns were well conserved across genotypes. However, a deeper analysis of distinct domains indicates that a subset of the HyperDs lost methylation in Het and Null oocytes and conversely, a subset of the HypoDs gained methylation in Het and Null oocytes. When we agnostically examined regions with differential methylation between the genotypes using a 10-kb tiling approach, we found 977 DMRs in Het compared to WT oocyte pools and 2300 DMRs in *Nlrp2*-null oocytes compared to WT oocytes. We noted that compared to WT, *Nlrp2*-null and Het gained DMRs in intergenic regions than in promoters, exons, or introns. None of these observed methylation changes favored any specific chromosomes, indicating that there are genome-wide imbalances in DNA methylation in both Het and *Nlrp2*-null oocytes. It remains to be determined whether this is causally related to the mislocalization of DNMT1 or other epigenetic regulators that influence DNA methylation.

Transcriptome profiling of GV oocytes and 2-cell embryos revealed interesting findings as well. *First*, the number of expressed genes was significantly lower in the *Nlrp2*-null GV oocytes but this difference was not observed in the transcriptome of 2-cell embryos which suggests that NLRP2 plays a critical role in maintaining the maternal transcriptome during oocyte maturation. However, the embryo may have mechanisms to partially compensate for the loss of NLRP2 by the 2-cell stage, possibly through the activation of zygotic transcription or other compensatory pathways. This highlights the importance of NLRP2 in the early stages of oocyte development and suggests that its role may be less critical once ZGA is underway. *Second*, many important epigenetic regulators were found among DEGs in *Nlrp2*-null oocytes and Het maternal effect embryos, including ZFP57, TRIM28, UHRF1, and KDM1B. We also identified some of the factors involved in oocyte transcriptome shaping among overexpressed DEGs such as CPEB1. We further found that other proteins of the SCMC, including TLE6, ZBED3, and PADI6 among the overexpressed genes. *Third*, with respect to overall transcriptome profiling results, we propose that altered RNA abundance could either reflect overexpression at an earlier stage, increased abundance due to increased transcript stability, delayed clearance of maternal transcriptome, or a combination of these. This could be related to changes in cytoplasmic lattices (CPLs) in *Nlrp2*-null oocytes. It is well established that oocytes store mRNAs and proteins that are essential for embryonic development. These include regulators of the epigenetic reprogramming that takes place in the early preimplantation embryo after fertilization and before the embryo activates its own biparental genome. These proteins localize to CPLs, which are twisted fibers

of individually stacked filaments, and of which the SCMC is a component [19]. The presence of an intact SCMC is vital to the integrity of the CPLs and for preventing premature degradation or premature nuclear localization of stored proteins and consequent early embryo arrest [24, 30, 33, 34]. If the disrupted CPLs cause altered protein abundance in the cell, the expression changes could be to compensate for lost or mislocalized proteins, for example, increased shuttling into the nucleus. We have shown that loss of maternal NLRP2 alters cytoplasmic localization of DNMT1 [28]. Knockout models of *Padi6*, *Nlrp14*, and *Stella* [47, 58, 68, 69] also have mislocalized DNMT1 along with its cofactor UHRF1, with aberrant nuclear localization of the DNMT1/UHRF1 complex, coupled with global hypermethylation and impeded ZGA [58, 68, 69]. DNMT1 is a known maintenance methyltransferase [70], but it can also function as a de novo methyltransferase [13, 68]. This may in part explain the altered methylation seen in *Nlrp2*-null and Het oocytes in this study, as well as our previous report of abnormal DNA methylation in embryos [28]. Additionally, we observed overexpression of UHRF1 in Het maternal effect embryos, which could represent a mechanism employed by the embryo to counteract the effects of the absence of NLRP2 and CPLs on DNMT1 localization. *Fourth*, transcriptome profiling of embryos revealed underexpression of many ZGA genes in Het maternal effect 2-cell embryos compared to both WT and Het paternal effect embryos. Although both minor ZGA and major ZGA were repressed, we observed that early 2-cell marker genes, specifically *Dux* family members, were normally expressed. In contrast, DUX target genes such as *Zscan4c*, *Zscan4 d*, and *Trim43* [71, 72] were underexpressed in Het maternal effect embryos, suggesting that maternal loss of NLRP2 mostly affects major ZGA during the late 2-cell stage. This finding aligns with previous studies on maternal *Nlrp14*-null and *Padi6*-null models, where major ZGA impairment was accompanied by developmental delay [47, 58]. *Fifth*, during MZT, maternal mRNA clearance occurs through two pathways: the maternal pathway (M-decay) before ZGA and the zygotic pathway (Z-decay), which requires ZGA and is regulated by polyA-binding protein genes, PABPN1 and PABPC1 [73]. In our study, *Pabpc1* was underexpressed, which may explain why M-decay genes were compensatorily overexpressed.

The final important step was the integrative analysis of transcriptome and methylome, to begin to shed light on whether altered transcription was at the origin of the methylation changes in the Het and Null oocytes. The lack of correlation indicates that this is likely not the case and that the methylome and transcriptome are disrupted through different mechanisms in these mutant oocytes.

Conclusion

Our study reveals a significant role for the maternal effect gene *Nlrp2* in shaping the transcriptome of GV oocytes, likely through a mechanism unrelated to DNA methylation establishment. We also showed that not only its absence in *Nlrp2*-null animals but also its reduced dosage in Het animals result in morphological and methylation differences in GV oocytes. Furthermore, extensive transcriptome changes in Het maternal effect embryos highlight the role of NLRP2 in early embryogenesis. These alteration affects regulators of the ZGA process, which may explain, at least in part, the adverse developmental outcomes observed in *Nlrp2*-null female mice.

Materials and methods

Oocytes and embryos collection and biological replicates

All experiments were approved by the Institutional Animal Care and Use Committee (IACUC) at Baylor College of Medicine (BCM) under study protocol (AN-2035) and conducted according to institutional and governmental regulations concerning the ethical use of animals. Animals were housed in facilities approved by the Association for Assessment and Accreditation for Laboratory Animal Care International (AAALAC).

We collected fully grown germinal-vesicle (GV) oocytes from the ovaries of our previously generated $Nlrp2^{tm1a/tm1a}$ (*Nlrp2*-null), $Nlrp2^{tm1a/+}$ heterozygous (Het), and $Nlrp2^{+/+}$ (WT) virgin females at 26–28 days of age [28]. To avoid any transgenerational reproductive effects in Het females from a maternally inherited null allele, we only studied Het females that were offspring of crosses between $Nlrp2^{tm1a/+}$ females and $Nlrp2^{tm1a/tm1a}$ males. We mechanically released oocytes from ovaries using a fine needle [74] and denuded recovered oocytes from granulosa cells by gentle pipetting with 75 µm stripper tips (CooperSurgical, Inc., USA) in M2 medium (Sigma, Japan). We then washed clean oocytes twice in PBS and collected 60–80 oocytes from both ovaries combined from each female, which served as one biological replicate oocyte pool. We lysed oocyte pools in 5 µl RLT Plus buffer (Qiagen, Germany) and stored them at −80 °C until further use.

2-cell embryos were collected following a superovulation treatment. Superovulation was induced in 4-week-old WT and *Nlrp2*-null mice by intraperitoneal injection of 5 units (U) of pregnant mare's serum gonadotropin (PMSG; Fisher Scientific, USA) followed by injection of 5 U of human chorionic gonadotropin (hCG; EMD Millipore, USA) 48 h (h) later. Immediately after hCG injection, females were mated with males. To collect the 2-cell embryos, we set up the following matings: (a.) The 11 WT embryos, which served as controls, were isolated from three WT females mated with three WT males.

Two matings yielded four embryos, and one mating yielded three embryos. (b.) The ten "Het paternal effect" embryos were isolated from three WT females mated with three *Nlrp2*-null males, with the null allele transmitted by the male. Two matings yielded three embryos, and one mating yielded four embryos. (c.) The ten "Het maternal effect" embryos were isolated from three *Nlrp2*-null females mated with three WT males, with the null allele transmitted by the female. Two matings yielded three embryos and one mating yielded four embryos (Supplementary Fig. 6A). Vaginal plug checks were performed the following morning, with midday of that day considered as E0.5. Two-cell embryos were collected at midday on E1.5. Embryos that had extruded the second polar body and formed two pronuclei were isolated in M2 medium (Sigma, Japan) by rupturing the oviduct ampullae. We lysed 2-cell embryos individually in 5 µl RLT Plus buffer (Qiagen, Germany) and stored them at − 80 °C until further use.

Histological studies

Ovaries were collected from 3-week-old mice, dissected from surrounding fat in 1X PBS and fixed in Formalde-Fresh (Fisher Scientific, Pittsburg, PA) overnight at 4 °C. Fixed tissues were washed twice for 30 min in 1X PBS and subsequently dehydrated in 50%, 70% ethanol, and 3× in 100% ethanol, for an hour each at room temperature (RT). The tissues were then treated 3× for 30 min each with xylene, followed by 2× 1 h in paraffin at 55 °C before embedding tissues in paraffin. Paraffin-embedded tissues were then serially sectioned at 5–8 µM thicknesses and used for hematoxylin and eosin staining (H&E) and microscopy to assess oocyte and follicle morphology. Every 10th section was photographed, and the number and developmental stages of follicles containing oocytes within each section were recorded. Five females from each genotype (*Nlrp2*-null, Het, and WT) were used for the analysis.

Parallel bisulfite and RNA sequencing by genomes and transcriptomes sequencing (G&T-seq)

To perform parallel bisulfite and RNA sequencing from the same thawed oocyte-pool lysate, we completed the initial 53 steps of the published G&T-seq protocol with minor changes to obtain gDNA and RNA from each oocyte pool [75]. Purified gDNA was then used for BS conversion and PBAT library preparation according to the described protocol [76] with minor changes. We first prepared MyOne Streptavidin C1 Dynabeads (Fisher Scientific, USA) according to manufacturer's instructions, labeled them with biotinylated oligo-dT30 VN (100 µM) to make the RNA libraries. We then resuspended the oligo-dT30 VN labeled Dynabeads into bead resuspension buffer before adding them to the tubes containing the cell lysates. We placed the tubes on a magnet to physically separate polyadenylated mRNA attached to the beads and gDNA in the supernatant. We transferred the supernatant containing the gDNA to a new tube and washed the Dynabeads three more times in wash buffer to maximize the gDNA recovery. To make the RNA-Seq libraries, we reverse-transcribed the polyadenylated mRNA attached to the Dynabeads and PCR-amplified the obtained cDNA before tagmentation-based cDNA library preparation with Illumina's Nextera XT Index Kit v2 Set C per the manufacturer's instructions. Briefly, we subjected 200 picograms of amplified cDNA underwent tagmentation at 55 °C for 5 min and mixed them with 1 µl of index 1 (one of S513, S515, to S518, S520 to S522) and 1 µl of index 2 (one of N701 to N707, N710 to N712, N714, N715). We then PCR-amplified and purified these products on Agencourt AMPure XP beads (Beckman Coulter, USA) in a 0.7:1 volumetric ratio and eluted them in nuclease-free water. To make the PBAT libraries, we purified the gDNA with Agencourt AMPure XP beads in a 0.9:1 volumetric ratio to capture gDNA fragments of > 200 bp. We then bisulfite-converted the recovered gDNA using the EZ Methylation Direct Kit (Zymo Research, USA) per manufacturer's instructions and double-tagged the converted DNA with Illumina adapters. To add the 6 NF oligo or Preamp Oligo (IDT, USA) which acts as Illumina adaptor one to the bisulfite-converted DNA, we eluted the gDNA fragments in 40 µl of first-strand synthesis master mix purified this first-strand synthesis product in a 0.8:1 volumetric ratio of Agencourt AMPure XP beads (Beckman Coulter, USA). We then added 40U of exonuclease I (New England Biolabs, USA) to the reactions for exonuclease digestion and eluted this product in 50 µl of second-strand synthesis master mix to add the 6 NR oligo or Adaptor 2 Oligo (IDT, USA) (which acts as Illumina adaptor two) by second-strand synthesis. We purified this product in a 0.8:1 volumetric ratio of Agencourt AMPure XP beads (Beckman Coulter, USA). Both amplifications were mediated by 50U of Klenow exo- (Enzymatics, USA). We next added a 50 µl PCR master mix with the Illumina forward PE1.0 primer and Illumina reverse indexed primer (iPCRTag) to the beads to amplify the libraries using 1U of KAPA Hifi Hotstart DNA polymerase (Roche, Switzerland). We then purified the libraries with a 0.8:1 volumetric ratio of Agencourt AMPure XP beads (Beckman Coulter, USA) and eluted them in EB buffer for storage at − 20 °C until sequencing.

Construction of libraries from 2-cell embryos

To make the RNA libraries from individual 2-cell embryos, we followed the SMART-Seq2 protocol [77]. The protocol incorporates the initial steps of G&T-seq

protocol, including labeling MyOne Streptavidin C1 Dynabeads with biotinylated oligo-dT30 VN, reverse transcription, PCR amplification, and tagmentation-based cDNA library preparation.

For all library preparations the composition of master mixes, programs used for amplifications and primer sequences are shown in Supplementary Table 16.

Validations by qRT-PCR

Total RNA from four pools of 50–80 GV oocytes from each experimental group was reverse-transcribed using the qScript cDNA SuperMix (Quanta Biosciences #95048). Quantitative RT-PCR of reverse-transcribed cDNAs was done with PerfeCTa® SYBR® Green FastMix ROX (Quanta Biosciences #95073) using the following primers: Nlrp2RTFor: 5′-AACACTGAGCCTGAAACA CTTGGA-3′, Nlrp2RTRev: 5′-CAGTTCAGTGGAGTG ATGGAGCA-3′, Trim28RTFor: 5′-GCACTGGACCAT GACCAAAATT-3′, Trim28RTRev: 5′-CAGAGCCCA AGAGGCAAAAC-3′, Obox3RTFor: 5′-TCCTGGTTC CATACCTGTTGTT-3′, Obox3RTRev: 5′-GCAGGT ATTCTTGGTATTCTTGG-3′. Gene expression analysis was performed using the ΔΔCt method and normalized to the expression of *Rpl19* mRNA.

Data processing

RNA-seq data processing and differential expression analysis

We conducted analysis on a total of 12 GV oocytes and 31 2-cell embryo libraries. Quality control (QC) of the raw reads was performed using FastQC [78], followed by Read Processing of adapters and quality trimming using Trim Galore [79]. Trimmed sequences were aligned to the Genome Reference Consortium mouse genome build 38 (GRCm38) with HiSat2 version 2.1.0 [80] in single-end mode. The GV oocyte data were quantified in SeqMonk and analyzed in Rstudio. We excluded reads aligning within unknown non-canonical splice junctions and quantitated RNA-seq data by counting reads crossing known and annotated splice junctions in the gene by building a canonical_splice_count.py tool. To run the program, we provided BAM files from a spliced alignment program (HiSat2) and a GTF file of gene annotations (GRCm38). As the program necessitates an exact match between observed splice and the position of the intron, we provided the same GTF file to the aligner when running the alignment. The program generates two output files: a Stats file, the details of which are presented in Supplementary Table 8, and a raw count matrix file suitable for input into DESeq2. The 2-cell embryo data were quantified in STAR_Salmon and analyzed in Rstudio. The program generates two output files: a Stats file, the details of which are presented in Supplementary Table 8, and a raw count matrix file suitable for input into DESeq2. For both GV oocytes and 2-cell embryo data, differential expression analysis was conducted using DESeq2 version 1.42.0 [81]. Genes were considered differentially expressed using a Wald test and based on a threshold of an adjusted p value <0.05 and $|\log^2\text{FoldChange}|> 1$. We additionally utilized the plotMA function to showcase the $\log^2$ fold changes associated with the mean of normalized counts for all the genotypes in the dataset.

To compare the transcriptome of WT GV oocytes and WT 2-cell embryos, we utilized the count matrix of WT GV oocytes and compared it to the count matrix of 2-cell embryos. To investigate the role of DEGs in ZGA, we compared our reference list with the list published by Wang and colleagues [54]. In that paper, authors defined zygote minor ZGA genes by comparing the transcriptome between DRB-treated zygote (DRB: 5,6-dichloro-1-B-D-ribofuranosyl-benzimidazol is a reversible inhibitor of RNA polymerase II) and control zygote. Early 2-cell minor ZGA was obtained by comparing the transcriptome between DRB-treated early 2-cell and control early 2-cell. Major ZGA was defined as overexpressed genes between late 2-cell and zygotes. Maternal decay genes were defined by combining the underexpressed genes of zygote versus MII oocyte, early 2-cell versus MII oocyte, late 2-cell versus MII oocyte, and 4-cell versus MII oocyte.

PBAT data processing and differential methylation analysis

Methylation sequencing data were processed using the standardized and reproducible processing pipeline nf-core/methylseq version 1.6.1 [82, 83] inside of Docker containers orchestrated by the workflow manager Nextflow version 23.11.0 [84]. Briefly, the processing pipeline consisted of sequencing Read QC using FastQC [78] followed by adapter sequence trimming using Trim Galore [79]. Trimmed reads were then aligned to the pre-indexed reference genome mm10 using bowtie2 [85]. Read alignments were then deduplicated, and methylation calls were extracted, reported, and converted into coverage2cytosine reports using Bismark [86] with the –pbat flag parameter, followed by Alignment QC using Qualimap [87]. All logs, summary tables, and quality control reports were agglomerated into a final report using MultiQC [88]. Coverage2cytosine reports were then imported into R version 4.3.0, converted into a methylRawList object using a 1 ×minimum coverage threshold cutoff using methylkit [89]. Downstream analyses were conducted using methylkit and consisted of filtering by Coverage (lo.count =1, lo.perc =0.1, hi.perc =99.9), Pearson correlation comparisons within treatment groups, ascertaining percent methylation for PCA analysis, and calculating differential methylation statistics

between groups using either logistic regression test or Fisher's exact test with McCullagh and Nelder correction for overdispersion and adjustment of p value significance using Benjamini–Hochberg multiple test correction.

Supplementary Information

The online version contains supplementary material available at https://doi.org/10.1186/s13148-025-01889-x.

Additional file 1
Additional file 2
Additional file 3
Additional file 4
Additional file 5
Additional file 6
Additional file 7
Additional file 8
Additional file 9
Additional file 10
Additional file 11
Additional file 12
Additional file 13
Additional file 14
Additional file 15
Additional file 16
Additional file 17
Additional file 18
Additional file 19
Additional file 20
Additional file 21
Additional file 22
Additional file 23
Additional file 24

Acknowledgements
We are grateful for the guidance provided by the following individuals at various stages of experiment execution and data analysis: Dr. Zhandong Liu, Dr. Elena Ivanova, Dr. Stephen Clark, and Dr. Antonio Galvao. Additionally, we would like to acknowledge the services provided by Neuropathology core at NRI for their assistance in ovary embedding and sectioning, as well as the Genomic and RNA Profiling Core at Baylor College of Medicine with funding from the NIH S10 grant (1S10OD023469) for performing Next Generation Sequencing.

Author contributions
IV and GK conceived the experiments; ZA, AKT, IC, and MS performed experiments; and MDJ, SA, ZA, MCM, and YWW analyzed data. HD and DCK provided essential guidance on optimal experiment execution, interpretation of data and data processing, as well as troubleshooting. ZA and IV wrote the manuscript. All authors contributed to manuscript editing. IV acquired funding and was responsible for final editing.

Funding
This work was supported by Grants R01HD092746 and P50HD103555 (neuropathology core), from the *Eunice Kennedy Shriver* National Institute of Child Health & Human Development of the National Institutes of Health. Dr. Michael Jochum received support from the Texas Children's Research Scholar Program. Dr. Momal Sharif was supported by a postdoctoral fellowship under National Research Service Award (NRSA) postdoctoral fellowshipT32HD098068. Dr. Hannah Demond was supported by Fondecyt postdoctoral fellowship 3200676.

Availability of data and materials
Data are provided within the manuscript or supplementary information files.

Declarations

Ethics approval and consent to participate
There is no human participant in this study. All experiments were approved by the Institutional Animal Care and Use Committee (IACUC) at Baylor College of Medicine (BCM) under study protocol (AN-2035) and conducted according to institutional and governmental regulations concerning the ethical use of animals.

Consent for publication
Not applicable.

Competing interests
The authors declare that they have no competing interests.

Author details
[1]Department of Obstetrics and Gynecology, Baylor College of Medicine, Houston, TX, USA. [2]Duncan Neurological Research Institute, Texas Children's Hospital, Houston, TX, USA. [3]Texas Children's Hospital, Houston, TX, USA. [4]Epigenetics Programme, Babraham Institute, Cambridge, UK. [5]Laboratory of Integrative Biology (LIBi), Centro de Excelencia en Medicina Traslacional (CEMT), Scientific and Technological Bioresource Nucleus (BIOREN), Universidad de la Frontera, Temuco, Chile. [6]Millennium Institute on Immunology and Immunotherapy, Santiago, Chile. [7]Biomedical Research Consortium (BMRC), Santiago, Chile. [8]Genomic and RNA Profiling Core, Baylor College of Medicine, Houston, TX, USA. [9]Bioinformatics Group, Babraham Institute, Cambridge, UK. [10]Loke Centre for Trophoblast Research, University of Cambridge, Cambridge, UK. [11]Wellcome-MRC Institute of Metabolic Science-Metabolic Research Laboratories, Cambridge, UK. [12]Department of Molecular and Human Genetics, Baylor College of Medicine, Houston, TX, USA.

Received: 4 February 2025 Accepted: 23 April 2025
Published online: 03 June 2025

References

1. Lucifero D, La Salle S, Bourc'his D, Martel J, Bestor TH, Trasler JM. Coordinate regulation of DNA methyltransferase expression during oogenesis. BMC Dev Biol. 2007;7:36.
2. Winata CL, Korzh V. The translational regulation of maternal mRNAs in time and space. FEBS Lett. 2018;592(17):3007–23.
3. Lee MT, Bonneau AR, Giraldez AJ. Zygotic genome activation during the maternal-to-zygotic transition. Annu Rev Cell Dev Biol. 2014;30:581–613.
4. Li L, Zheng P, Dean J. Maternal control of early mouse development. Development. 2010;137(6):859–70.
5. Aoki F. Zygotic gene activation in mice: profile and regulation. J Reprod Dev. 2022;68(2):79–84.
6. Chotalia M, Smallwood SA, Ruf N, Dawson C, Lucifero D, Frontera M, James K, Dean W, Kelsey G. Transcription is required for establishment of germline methylation marks at imprinted genes. Genes Dev. 2009;23(1):105–17.
7. Veselovska L, Smallwood SA, Saadeh H, Stewart KR, Krueger F, Maupetit-Mehouas S, Arnaud P, Tomizawa S, Andrews S, Kelsey G. Deep sequencing and de novo assembly of the mouse oocyte transcriptome define the contribution of transcription to the DNA methylation landscape. Genome Biol. 2015;16:209.
8. Kobayashi H, Sakurai T, Imai M, Takahashi N, Fukuda A, Yayoi O, Sato S, Nakabayashi K, Hata K, Sotomaru Y, et al. Contribution of intragenic DNA

methylation in mouse gametic DNA methylomes to establish oocyte-specific heritable marks. PLoS Genet. 2012;8(1):e1002440.
9. Demond H, Khan S, Castillo-Fernandez J, Hanna CW, Kelsey G. Transcriptome and DNA methylation profiling during the NSN to SN transition in mouse oocytes. BMC Mol Cell Biol. 2025;26(1):2.
10. Stewart KR, Veselovska L, Kelsey G. Establishment and functions of DNA methylation in the germline. Epigenomics. 2016;8(10):1399–413.
11. Stewart KR, Veselovska L, Kim J, Huang J, Saadeh H, Tomizawa S, Smallwood SA, Chen T, Kelsey G. Dynamic changes in histone modifications precede de novo DNA methylation in oocytes. Genes Dev. 2015;29(23):2449–62.
12. Smallwood SA, Tomizawa S, Krueger F, Ruf N, Carli N, Segonds-Pichon A, Sato S, Hata K, Andrews SR, Kelsey G. Dynamic CpG island methylation landscape in oocytes and preimplantation embryos. Nat Genet. 2011;43(8):811–4.
13. Shirane K, Toh H, Kobayashi H, Miura F, Chiba H, Ito T, Kono T, Sasaki H. Mouse oocyte methylomes at base resolution reveal genome-wide accumulation of non-CpG methylation and role of DNA methyltransferases. PLoS Genet. 2013;9(4):e1003439.
14. Gahurova L, Tomizawa SI, Smallwood SA, Stewart-Morgan KR, Saadeh H, Kim J, Andrews SR, Chen T, Kelsey G. Transcription and chromatin determinants of de novo DNA methylation timing in oocytes. Epigenet Chromatin. 2017;10:25.
15. Anvar Z, Chakchouk I, Demond H, Sharif M, Kelsey G, Van den Veyver IB. DNA methylation dynamics in the female germline and maternal-effect mutations that disrupt genomic imprinting. Genes (Basel). 2021;12(8):1214.
16. Proudhon C, Duffie R, Ajjan S, Cowley M, Iranzo J, Carbajosa G, Saadeh H, Holland ML, Oakey RJ, Rakyan VK, et al. Protection against de novo methylation is instrumental in maintaining parent-of-origin methylation inherited from the gametes. Mol Cell. 2012;47(6):909–20.
17. Soellner L, Begemann M, Mackay DJ, Gronskov K, Tumer Z, Maher ER, Temple IK, Monk D, Riccio A, Linglart A, et al. Recent advances in imprinting disorders. Clin Genet. 2017;91(1):3–13.
18. Kaneda M, Hirasawa R, Chiba H, Okano M, Li E, Sasaki H. Genetic evidence for Dnmt3a-dependent imprinting during oocyte growth obtained by conditional knockout with Zp3-Cre and complete exclusion of Dnmt3b by chimera formation. Genes Cells. 2010;15(3):169–79.
19. Jentoft IMA, Bauerlein FJB, Welp LM, Cooper BH, Petrovic A, So C, Penir SM, Politi AZ, Horokhovskyi Y, Takala I, et al. Mammalian oocytes store proteins for the early embryo on cytoplasmic lattices. Cell. 2023;186(24):5308–27.
20. Bebbere D, Albertini DF, Coticchio G, Borini A, Ledda S. The subcortical maternal complex: emerging roles and novel perspectives. Mol Hum Reprod. 2021;27(7):gaab043.
21. Bebbere D, Masala L, Albertini DF, Ledda S. The subcortical maternal complex: Multiple functions for one biological structure? J Assist Reprod Genet. 2016;33(11):1431–8.
22. Monk D, Sanchez-Delgado M, Fisher R. NLRPs, the subcortical maternal complex and genomic imprinting. Reproduction. 2017;154(6):R161–70.
23. Chi P, Ou G, Qin D, Han Z, Li J, Xiao Q, Gao Z, Xu C, Qi Q, Liu Q, et al. Structural basis of the subcortical maternal complex and its implications in reproductive disorders. Nat Struct Mol Biol. 2024;31(1):115–24.
24. Li L, Baibakov B, Dean J. A subcortical maternal complex essential for preimplantation mouse embryogenesis. Dev Cell. 2008;15(3):416–25.
25. Yu XJ, Yi Z, Gao Z, Qin D, Zhai Y, Chen X, Ou-Yang Y, Wang ZB, Zheng P, Zhu MS, et al. The subcortical maternal complex controls symmetric division of mouse zygotes by regulating F-actin dynamics. Nat Commun. 2014;5:4887.
26. Tong ZB, Gold L, Pfeifer KE, Dorward H, Lee E, Bondy CA, Dean J, Nelson LM. Mater, a maternal effect gene required for early embryonic development in mice. Nat Genet. 2000;26(3):267–8.
27. Tashiro F, Kanai-Azuma M, Miyazaki S, Kato M, Tanaka T, Toyoda S, Yamato E, Kawakami H, Miyazaki T, Miyazaki J. Maternal-effect gene Ces5/Ooep/Moep19/Floped is essential for oocyte cytoplasmic lattice formation and embryonic development at the maternal-zygotic stage transition. Genes Cells. 2010;15(8):813–28.
28. Mahadevan S, Sathappan V, Utama B, Lorenzo I, Kaskar K, Van den Veyver IB. Maternally expressed NLRP2 links the subcortical maternal complex (SCMC) to fertility, embryogenesis and epigenetic reprogramming. Sci Rep. 2017;7:44667.
29. Zheng P, Dean J. Role of Filia, a maternal effect gene, in maintaining euploidy during cleavage-stage mouse embryogenesis. Proc Natl Acad Sci U S A. 2009;106(18):7473–8.
30. Esposito G, Vitale AM, Leijten FP, Strik AM, Koonen-Reemst AM, Yurttas P, Robben TJ, Coonrod S, Gossen JA. Peptidylarginine deiminase (PAD) 6 is essential for oocyte cytoskeletal sheet formation and female fertility. Mol Cell Endocrinol. 2007;273(1–2):25–31.
31. Ohsugi M, Zheng P, Baibakov B, Li L, Dean J. Maternally derived FILIA-MATER complex localizes asymmetrically in cleavage-stage mouse embryos. Development. 2008;135(2):259–69.
32. Peng H, Chang B, Lu C, Su J, Wu Y, Lv P, Wang Y, Liu J, Zhang B, Quan F, et al. Nlrp2, a maternal effect gene required for early embryonic development in the mouse. PLoS ONE. 2012;7(1):e30344.
33. Gao Z, Zhang X, Yu X, Qin D, Xiao Y, Yu Y, Xiang Y, Nie X, Lu X, Liu W, et al. Zbed3 participates in the subcortical maternal complex and regulates the distribution of organelles. J Mol Cell Biol. 2018;10(1):74–88.
34. Qin D, Gao Z, Xiao Y, Zhang X, Ma H, Yu X, Nie X, Fan N, Wang X, Ouyang Y, et al. The subcortical maternal complex protein Nlrp4f is involved in cytoplasmic lattice formation and organelle distribution. Development. 2019;146(20):dev183616.
35. Kanzaki S, Tamura S, Ito T, Wakabayashi M, Saito K, Kato S, Ohta Y, Sekita Y, Kimura T. Involvement of Nlrp9a/b/c in mouse preimplantation development. Reproduction. 2020;160(2):181–91.
36. Zhu K, Yan L, Zhang X, Lu X, Wang T, Yan J, Liu X, Qiao J, Li L. Identification of a human subcortical maternal complex. Mol Hum Reprod. 2015;21(4):320–9.
37. Xu Y, Shi Y, Fu J, Yu M, Feng R, Sang Q, Liang B, Chen B, Qu R, Li B, et al. Mutations in PADI6 cause female infertility characterized by early embryonic arrest. Am J Hum Genet. 2016;99(3):744–52.
38. Alazami AM, Awad SM, Coskun S, Al-Hassan S, Hijazi H, Abdulwahab FM, Poizat C, Alkuraya FS. TLE6 mutation causes the earliest known human embryonic lethality. Genome Biol. 2015;16:240.
39. Parry DA, Logan CV, Hayward BE, Shires M, Landolsi H, Diggle C, Carr I, Rittore C, Touitou I, Philibert L, et al. Mutations causing familial biparental hydatidiform mole implicate c6orf221 as a possible regulator of genomic imprinting in the human oocyte. Am J Hum Genet. 2011;89(3):451–8.
40. Docherty LE, Rezwan FI, Poole RL, Turner CL, Kivuva E, Maher ER, Smithson SF, Hamilton-Shield JP, Patalan M, Gizewska M, et al. Mutations in NLRP5 are associated with reproductive wastage and multilocus imprinting disorders in humans. Nat Commun. 2015;6:8086.
41. Murdoch S, Djuric U, Mazhar B, Seoud M, Khan R, Kuick R, Bagga R, Kircheisen R, Ao A, Ratti B, et al. Mutations in NALP7 cause recurrent hydatidiform moles and reproductive wastage in humans. Nat Genet. 2006;38(3):300–2.
42. Arian S, Rubin J, Chakchouk I, Sharif M, Mahadevan SK, Erfani H, Shelly K, Liao L, Lorenzo I, Ramakrishnan R, et al. Reproductive outcomes from maternal loss of Nlrp2 are not improved by IVF or embryo transfer consistent with oocyte-specific defect. Reprod Sci. 2021;28(7):1850–65.
43. Anvar Z, Chakchouk I, Sharif M, Mahadevan S, Nasiotis ET, Su L, Liu Z, Wan YW, Van den Veyver IB. Loss of the maternal effect gene Nlrp2 alters the transcriptome of ovulated mouse oocytes and impacts expression of histone demethylase KDM1B. Reprod Sci. 2023;30(9):2780–93.
44. Meyer E, Lim D, Pasha S, Tee LJ, Rahman F, Yates JR, Woods CG, Reik W, Maher ER. Germline mutation in NLRP2 (NALP2) in a familial imprinting disorder (Beckwith-Wiedemann Syndrome). PLoS Genet. 2009;5(3):e1000423.
45. Begemann M, Rezwan FI, Beygo J, Docherty LE, Kolarova J, Schroeder C, Buiting K, Chokkalingam K, Degenhardt F, Wakeling EL, et al. Maternal variants in NLRP and other maternal effect proteins are associated with multilocus imprinting disturbance in offspring. J Med Genet. 2018;55(7):497–504.
46. Demond H, Anvar Z, Jahromi BN, Sparago A, Verma A, Davari M, Calzari L, Russo S, Jahromi MA, Monk D, et al. A KHDC3L mutation resulting in recurrent hydatidiform mole causes genome-wide DNA methylation loss in oocytes and persistent imprinting defects post-fertilisation. Genome Med. 2019;11(1):84.

47. Giaccari C, Cecere F, Argenziano L, Galvao A, Acampora D, Rossi G, Mele BH, Cubellis MV, Cerrato F, Andrews S, Cecconi S (2024) A maternal-effect Padi6 variant results in abnormal nuclear localization of DNMT1 and failure of epigenetic reprogramming and zygotic genome activation in mouse embryos. Genes Dev
48. Canovas S, Ivanova E, Romar R, Garcia-Martinez S, Soriano-Ubeda C, Garcia-Vazquez FA, Saadeh H, Andrews S, Kelsey G, Coy P. DNA methylation and gene expression changes derived from assisted reproductive technologies can be decreased by reproductive fluids. Elife. 2017;6:e23670.
49. Miura F, Enomoto Y, Dairiki R, Ito T. Amplification-free whole-genome bisulfite sequencing by post-bisulfite adaptor tagging. Nucleic Acids Res. 2012;40(17):e136.
50. Kawai T, Richards JS, Shimada M. Large-scale DNA demethylation occurs in proliferating ovarian granulosa cells during mouse follicular development. Commun Biol. 2021;4(1):1334.
51. Illingworth RS, Gruenewald-Schneider U, Webb S, Kerr AR, James KD, Turner DJ, Smith C, Harrison DJ, Andrews R, Bird AP. Orphan CpG islands identify numerous conserved promoters in the mammalian genome. PLoS Genet. 2010;6(9):e1001134.
52. Landeira D, Bagci H, Malinowski AR, Brown KE, Soza-Ried J, Feytout A, Webster Z, Ndjetehe E, Cantone I, Asenjo HG, et al. Jarid2 coordinates nanog expression and PCP/Wnt signaling required for efficient ESC differentiation and early embryo development. Cell Rep. 2015;12(4):573–86.
53. Ji S, Chen F, Stein P, Wang J, Zhou Z, Wang L, Zhao Q, Lin Z, Liu B, Xu K, et al. OBOX regulates mouse zygotic genome activation and early development. Nature. 2023;620(7976):1047–53.
54. Wang M, Chen Z, Zhang Y. CBP/p300 and HDAC activities regulate H3K27 acetylation dynamics and zygotic genome activation in mouse preimplantation embryos. EMBO J. 2022;41(22):e112012.
55. Court F, Martin-Trujillo A, Romanelli V, Garin I, Iglesias-Platas I, Salafsky I, Guitart M, Perez de Nanclares G, Lapunzina P, Monk D. Genome-wide allelic methylation analysis reveals disease-specific susceptibility to multiple methylation defects in imprinting syndromes. Hum Mutat. 2013;34(4):595–602.
56. Fontana L, Bedeschi MF, Maitz S, Cereda A, Fare C, Motta S, Seresini A, D'Ursi P, Orro A, Pecile V, et al. Characterization of multi-locus imprinting disturbances and underlying genetic defects in patients with chromosome 11p15.5 related imprinting disorders. Epigenetics. 2018;13(9):897–909.
57. Tannorella P, Calzari L, Daolio C, Mainini E, Vimercati A, Gentilini D, Soli F, Pedrolli A, Bonati MT, Larizza L, et al. Germline variants in genes of the subcortical maternal complex and Multilocus Imprinting Disturbance are associated with miscarriage/infertility or Beckwith-Wiedemann progeny. Clin Epigenet. 2022;14(1):43.
58. Yan R, Cheng X, Gu C, Xu Y, Long X, Zhai J, Sun F, Qian J, Du Y, Wang H, et al. Dynamics of DNA hydroxymethylation and methylation during mouse embryonic and germline development. Nat Genet. 2023;55(1):130–43.
59. Zheng W, Hu H, Dai J, Zhang S, Gu Y, Dai C, Guo J, Xu X, Li Y, Zhang S, et al. Expanding the genetic and phenotypic spectrum of the subcortical maternal complex genes in recurrent preimplantation embryonic arrest. Clin Genet. 2021;99(2):286–91.
60. Rezaei M, Suresh B, Bereke E, Hadipour Z, Aguinaga M, Qian J, Bagga R, Fardaei M, Hemida R, Jagadeesh S, et al. Novel pathogenic variants in NLRP7, NLRP5, and PADI6 in patients with recurrent hydatidiform moles and reproductive failure. Clin Genet. 2021;99(6):823–8.
61. Eggermann T, Kadgien G, Begemann M, Elbracht M. Biallelic PADI6 variants cause multilocus imprinting disturbances and miscarriages in the same family. Eur J Hum Genet. 2021;29(4):575–80.
62. Uysal F, Ozturk S, Akkoyunlu G. Superovulation alters DNA methyltransferase protein expression in mouse oocytes and early embryos. J Assist Reprod Genet. 2018;35(3):503–13.
63. Ishikawa T, Tamai Y, Zorn AM, Yoshida H, Seldin MF, Nishikawa S, Taketo MM. Mouse Wnt receptor gene Fzd5 is essential for yolk sac and placental angiogenesis. Development. 2001;128(1):25–33.
64. Wang H, Zhong C, Yang R, Yin Y, Tan R, Gao L, Gao C, Cui Y, Pu D, Wu J. Hfm1 participates in Golgi-associated spindle assembly and division in mouse oocyte meiosis. Cell Death Dis. 2020;11(6):490.
65. Xie B, Zhang L, Zhao H, Bai Q, Fan Y, Zhu X, Yu Y, Li R, Liang X, Sun QY, et al. Poly(ADP-ribose) mediates asymmetric division of mouse oocyte. Cell Res. 2018;28(4):462–75.
66. Kurowski A, Molotkov A, Soriano P. FGFR1 regulates trophectoderm development and facilitates blastocyst implantation. Dev Biol. 2019;446(1):94–101.
67. Merrill BJ, Pasolli HA, Polak L, Rendl M, Garcia-Garcia MJ, Anderson KV, Fuchs E. Tcf3: a transcriptional regulator of axis induction in the early embryo. Development. 2004;131(2):263–74.
68. Li Y, Zhang Z, Chen J, Liu W, Lai W, Liu B, Li X, Liu L, Xu S, Dong Q, et al. Stella safeguards the oocyte methylome by preventing de novo methylation mediated by DNMT1. Nature. 2018;564(7734):136–40.
69. Uemura S, Maenohara S, Inoue K, Ogonuki N, Matoba S, Ogura A, Kurumizaka M, Yamagata K, Sharif J, Koseki H, et al. UHRF1 is essential for proper cytoplasmic architecture and function of mouse oocytes and derived embryos. Life Sci Alliance 2023;6(8).
70. Dahlet T, Argueso Lleida A, Al Adhami H, Dumas M, Bender A, Ngondo RP, Tanguy M, Vallet J, Auclair G, Bardet AF, et al. Genome-wide analysis in the mouse embryo reveals the importance of DNA methylation for transcription integrity. Nat Commun. 2020;11(1):3153.
71. Hu K, Li W, Ma S, Fang D, Xu J. The identification and classification of candidate genes during the zygotic genome activation in the mammals. Zygote. 2024;32(2):119–29.
72. De Iaco A, Planet E, Coluccio A, Verp S, Duc J, Trono D. DUX-family transcription factors regulate zygotic genome activation in placental mammals. Nat Genet. 2017;49(6):941–5.
73. Zhao LW, Zhu YZ, Wu YW, Pi SB, Shen L, Fan HY. Nuclear poly(A) binding protein 1 (PABPN1) mediates zygotic genome activation-dependent maternal mRNA clearance during mouse early embryonic development. Nucleic Acids Res. 2022;50(1):458–72.
74. Castillo-Fernandez J, Herrera-Puerta E, Demond H, Clark SJ, Hanna CW, Hemberger M, Kelsey G. Increased transcriptome variation and localised DNA methylation changes in oocytes from aged mice revealed by parallel single-cell analysis. Aging Cell. 2020;19(12):e13278.
75. Macaulay IC, Teng MJ, Haerty W, Kumar P, Ponting CP, Voet T. Separation and parallel sequencing of the genomes and transcriptomes of single cells using G&T-seq. Nat Protoc. 2016;11(11):2081–103.
76. Clark SJ, Smallwood SA, Lee HJ, Krueger F, Reik W, Kelsey G. Genome-wide base-resolution mapping of DNA methylation in single cells using single-cell bisulfite sequencing (scBS-seq). Nat Protoc. 2017;12(3):534–47.
77. Picelli S, Faridani OR, Bjorklund AK, Winberg G, Sagasser S, Sandberg R. Full-length RNA-seq from single cells using Smart-seq2. Nat Protoc. 2014;9(1):171–81.
78. A quality control tool for high throughput sequence data.
79. A wrapper tool around Cutadapt and FastQC to consistently apply quality and adapter trimming to FastQ files, with some extra functionality for MspI-digested RRBS-type (Reduced Representation Bisufite-Seq) libraries.
80. Kim D, Langmead B, Salzberg SL. HISAT: a fast spliced aligner with low memory requirements. Nat Methods. 2015;12(4):357–60.
81. Love MI, Huber W, Anders S. Moderated estimation of fold change and dispersion for RNA-seq data with DESeq2. Genome Biol. 2014;15(12):550.
82. Ewels P, Hüther P, Hammarén R, Peltzer A, etal. nf-core/methylseq: nf-core/methylseq version 1.6.1 [Nauseous Serpent]. 2021.
83. Ewels PA, Peltzer A, Fillinger S, Patel H, Alneberg J, Wilm A, Garcia MU, Di Tommaso P, Nahnsen S. The nf-core framework for community-curated bioinformatics pipelines. Nat Biotechnol. 2020;38(3):276–8.
84. Di Tommaso P, Chatzou M, Floden EW, Barja PP, Palumbo E, Notredame C. Nextflow enables reproducible computational workflows. Nat Biotechnol. 2017;35(4):316–9.
85. Langmead B, Salzberg SL. Fast gapped-read alignment with Bowtie 2. Nat Methods. 2012;9(4):357–9.
86. Krueger F, Andrews SR. Bismark: a flexible aligner and methylation caller for Bisulfite-Seq applications. Bioinformatics. 2011;27(11):1571–2.
87. Okonechnikov K, Conesa A, Garcia-Alcalde F. Qualimap 2: advanced multi-sample quality control for high-throughput sequencing data. Bioinformatics. 2016;32(2):292–4.
88. Ewels P, Magnusson M, Lundin S, Kaller M. MultiQC: summarize analysis results for multiple tools and samples in a single report. Bioinformatics. 2016;32(19):3047–8.

89. Akalin A, Kormaksson M, Li S, Garrett-Bakelman FE, Figueroa ME, Melnick A, Mason CE. methylKit: a comprehensive R package for the analysis of genome-wide DNA methylation profiles. Genome Biol. 2012;13(10):R87.

Publisher's Note